AD-A138 544 RAYLEIGH-TAYLOR INSTABILITY IN THE PRESENCE OF A STRATIFIED SHEAR LAYER(U) NAVAL RESEARCH LAB WASHINGTON DC P SATYANARAYANA ET AL. 16 FEB 84 NRL-MR-5263 1/1

UNCLASSIFIED F/G 4/1 NL

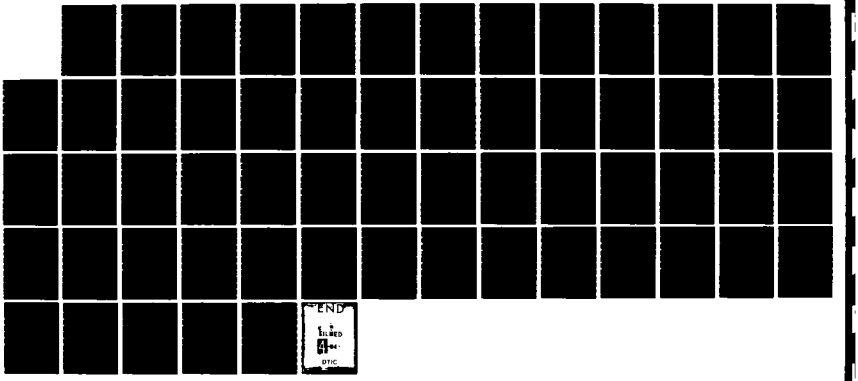

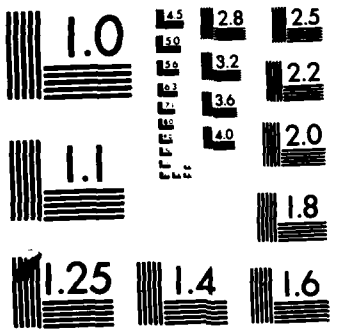

NRL Memorandum Report 5263

2

Rayleigh-Taylor Instability in the Presence of a Stratified Shear Layer

P. SATYANARAYANA AND P. N. GUZDAR

Science Applications, Inc.
McLean, VA 22102

J. D. HUBA AND S. L. OSSAKOW

Plasma Physics Division

February 16, 1984

This research was sponsored by the Defense Nuclear Agency under Subtask S99QMXBC, work unit 00067, work unit title "Plasma Structure Evolution," and by the Office of Naval Research.

NAVAL RESEARCH LABORATORY
Washington, D.C.

SECURITY CLASSIFICATION OF THIS PAGE

REPORT DOCUMENTATION PAGE

1a. REPORT SECURITY CLASSIFICATION UNCLASSIFIED	1b. RESTRICTIVE MARKINGS
2a. SECURITY CLASSIFICATION AUTHORITY	3. DISTRIBUTION/AVAILABILITY OF REPORT
2b. DECLASSIFICATION/DOWNGRADING SCHEDULE	Approved for public release; distribution unlimited.
4. PERFORMING ORGANIZATION REPORT NUMBER(S) NRL Memorandum Report 5263	5. MONITORING ORGANIZATION REPORT NUMBER(S)
6a. NAME OF PERFORMING ORGANIZATION Naval Research Laboratory 6b. OFFICE SYMBOL (If applicable)	7a. NAME OF MONITORING ORGANIZATION
6c. ADDRESS (City, State and ZIP Code) Washington, DC 20375	7b. ADDRESS (City, State and ZIP Code)
8a. NAME OF FUNDING/SPONSORING ORGANIZATION DNA and ONR 8b. OFFICE SYMBOL (If applicable)	9. PROCUREMENT INSTRUMENT IDENTIFICATION NUMBER
8c. ADDRESS (City, State and ZIP Code) Washington, DC 20305 Arlington, VA 22217	10. SOURCE OF FUNDING NOS. PROGRAM ELEMENT NO.: 62715H PROJECT NO.: RR033-02-44 TASK NO.: WORK UNIT NO.: 47-0889-0-4, 47-0883-0-4
11. TITLE (Include Security Classification) (See page ii)	
12. PERSONAL AUTHOR(S) P. Satyanarayana,* P.N. Guzdar,* J.D. Huba and S.L. Ossakow	
13a. TYPE OF REPORT Interim 13b. TIME COVERED FROM _____ TO _____	14. DATE OF REPORT (Yr., Mo., Day) February 16, 1984 15. PAGE COUNT 59
16. SUPPLEMENTARY NOTATION *Present address: Science Applications, Inc., McLean, VA 22102 This research was sponsored by the Defense Nuclear Agency under Subtask S99QMXBC, work unit 00067, work unit title "Plasma Structure Evolution," and by the Office of Naval Research.	
17. COSATI CODES FIELD / GROUP / SUB. GR.	18. SUBJECT TERMS (Continue on reverse if necessary and identify by block number) Rayleigh-Taylor instability Velocity shear Ionosphere Nonlocal theory

19. ABSTRACT (Continue on reverse if necessary and identify by block number)

A nonlocal theory of the Rayleigh-Taylor instability which includes the effect of a transverse velocity shear is presented. A two fluid model is used to describe an inhomogeneous plasma under the influence of gravity and sheared equilibrium flow velocity, and to derive a differential equation describing the generalized Rayleigh-Taylor instability. An extensive parametric study is made in the collisionless and collisional regime, and the corresponding dispersion curves are presented. The results are applied to the equatorial F region and to barium releases in the ionosphere.

20. DISTRIBUTION/AVAILABILITY OF ABSTRACT UNCLASSIFIED/UNLIMITED ☒ SAME AS RPT ☐ DTIC USERS ☐	21. ABSTRACT SECURITY CLASSIFICATION UNCLASSIFIED
22a. NAME OF RESPONSIBLE INDIVIDUAL P. Satyanarayana	22b. TELEPHONE NUMBER (Include Area Code) (202) 767-3630 22c. OFFICE SYMBOL Code 4780

DD FORM 1473, 83 APR EDITION OF 1 JAN 73 IS OBSOLETE.

SECURITY CLASSIFICATION OF THIS PAGE

11. TITLE

RAYLEIGH-TAYLOR INSTABILITY IN THE PRESENCE OF A STRATIFIED SHEAR LAYER

CONTENTS

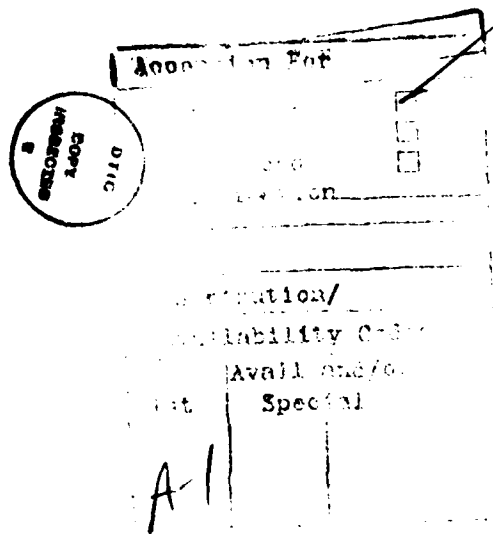

RAYLEIGH-TAYLOR INSTABILITY IN THE PRESENCE OF A STRATIFIED SHEAR LAYER

I. Introduction

The Rayleigh-Taylor instability (Rayleigh, 1894; Taylor, 1950) arises in a wide range of physical phenomena. This instability is primarily driven by a gravitational force acting on an inverted density gradient (e.g., a heavy fluid supported by a light fluid). In a magnetized plasma these modes can exist in both the collisionless and collisional domains. For example, theoretical models (Hudson and Kennel, 1975; Ossakow, 1979) and numerical simulations (Scannapieco and Ossakow, 1976; Ossakow et al., 1979; Zalesak and Ossakow, 1980; Zalesak et al., 1982) of the collisional Rayleigh-Taylor instability in the earth's ionosphere show that the mode evolves into plasma bubbles that extend upward from the bottomside to the topside of the F-layer. The collisionless interchange type instability (ballooning mode) can exist in the earth's plasmasphere (Vinas, 1980) as well as in laboratory plasmas (Coppi and Rosenbluth, 1966; Coppi et al., 1979). These collisionless modes arise due to an unfavorable curvature in the magnetic field (simulating an effective gravity) in the presence of a pressure gradient. This instability may also arise in the acceleration of a heavy fluid by one of lower density as in targets accelerated by laser ablation (Emery et al., 1982 and references therein) or the deceleration of barium clouds injected in the ionosphere (Pillip, 1971; Rosenberg, 1971; Davis et al., 1974; Fedder, 1980).

In some of the above situations, the equilibrium flow velocity is observed to be inhomogeneous. For example, in the ionosphere, the horizontal plasma velocity during equatorial spread F (ESF) reverses its direction as a function of altitude (Kudeki et al., 1981; Tsunoda, 1981a; Tsunoda and White, 1981; Kelley et al., 1981). In the plasmasphere, steep shear in the flow

Manuscript approved November 1, 1983.

velocity can exist due to the dominating corotating electric field inside the plasmasphere and a convective magnetospheric electric field penetrating across the plasmapause. This can lead to a Kelvin-Helmholtz type erosion of the outer edge of the plasmasphere (Viñas, 1980; Viñas and Madden, 1983). In targets accelerated by laser ablation, the Rayleigh-Taylor instability (Bodner, 1974) nonlinearly evolves into a bubble and spike structure (as during ESF) and developes a strong shear in the flow velocity (Harlow and Welsh, 1966; Daly, 1967; Emery et al., 1982). In the absence of any other driving mechanism, the velocity shear gives rise to a transverse Kelvin-Helmholtz instability in fluids (Kelvin, 1910; Chandrasekhar, 1961) and in magnetized plasmas (Mikhailovskii, 1974). All of the above examples suggest a need for a detailed study of configurations in which the two driving mechanisms co-exist, namely, inhomogeneous velocity flows and gravity (or similar forces).

The influence of velocity shear on interchange instabilities has been studied by Drazin (1958) and Chandrasekhar (1961) in the context of fluid models; by Hamieri (1979) in the context of laboratory plasmas; by Vinas (1980) in the context of the plasmasphere; and by Guzdar et al. (1982; 1983) in the context of equatorial spread F. In this paper we report on our detailed study of the influence of velocity shear on the collisionless and collisional Rayleigh-Taylor instability and apply the results to a variety of geophysical phenomena. We find that the velocity shear can have a dramatic effect on the Rayleigh-Taylor instability (Guzdar et al., 1982; 1983). A sufficiently strong velocity shear can stabilize the most unstable modes (i.e., those for which $kL > 1$ where L is the scale length of the inhomogeneity and k is the perpendicular wave number), which leads to maximum growth in the long wavelength regime (for which $kL < 1$). Thus velocity shear, in some

domains, preferentially excites a long wavelength mode, in sharp contrast to the behavior of the mode in the absence of velocity shear.

This paper is divided into five sections. In the next section, we derive the general mode structure equation describing an inhomogeneous collisional plasma which contains a sheared velocity flow and which is under the action of gravity. In the third section we discuss the stability of this plasma in two limits, namely, the Rayleigh-Taylor limit (no velocity shear), and the Kelvin-Helmholtz limit (no gravity). In the fourth section we present the results of the analysis of the generalized Rayleigh-Taylor instability, i.e., when both velocity shear and gravity are present. In the final section, we discuss the results and apply them to geophysical phenomena.

II. Theory

We consider an infinite slab of magnetized plasma. The coordinate system is shown in Fig. 1. The magnetic field is uniform and is in the $\hat{z}$ direction ($\underline{B} = B\,\hat{z}$), the acceleration due to gravity is in the x direction ($\underline{g} = -g\,\hat{x}$), the ambient electric field is inhomogeneous and is in the x direction ($\underline{E}_0 = E_0(x)\,\hat{x}$), and the density is inhomogeneous in the x direction ($n_0 = n_0(x)$). The inhomogeneity in the background electric field leads to a sheared equilibrium flow, $\underline{V}_0(x) = -c\,E_0(x)/B\,\hat{y}$.

The basic assumptions used in the analysis are as follows: (1) the perturbed quantities vary as $\delta p \sim \delta p(x) \exp[i(k_y y - \omega t)]$, where k_y is the wave number along y direction and $\omega = \omega_r + i\gamma$, implying growth for $\gamma > 0$; (2) the ordering in the frequencies is such that $\omega, \nu_{in} \ll \Omega_i$, where ν_{in} is the ion-neutral collision frequency and Ω_i is the ion-gyro-frequency; (3) we ignore finite-gyroradius effects by limiting the wavelength domain to $k\rho_i \ll 1$, where ρ_i is the mean ion-Larmor radius; (4) we neglect perturbations along the magnetic field ($k_\parallel = 0$) so that only two dimensional mode structure in the x-y plane is obtained; (5) we retain ion inertia effects, thereby including the ion polarization drift, but ignore electron inertia; and (6) we neglect ion and electron pressure.

A key feature of our analysis is that a nonlocal theory is developed. That is, the mode structure of the potential in the x direction, the direction in which density and the flow velocity are assumed to vary, is determined by a differential equation rather than an algebraic equation obtained by Fourier analysis. This technique allows one to study modes which have wavelengths comparable to the scale size of the inhomogeneities (i.e., $k_y L < 1$, where L represents scale lengths of the boundary layer). In fact, nonlocal theory is

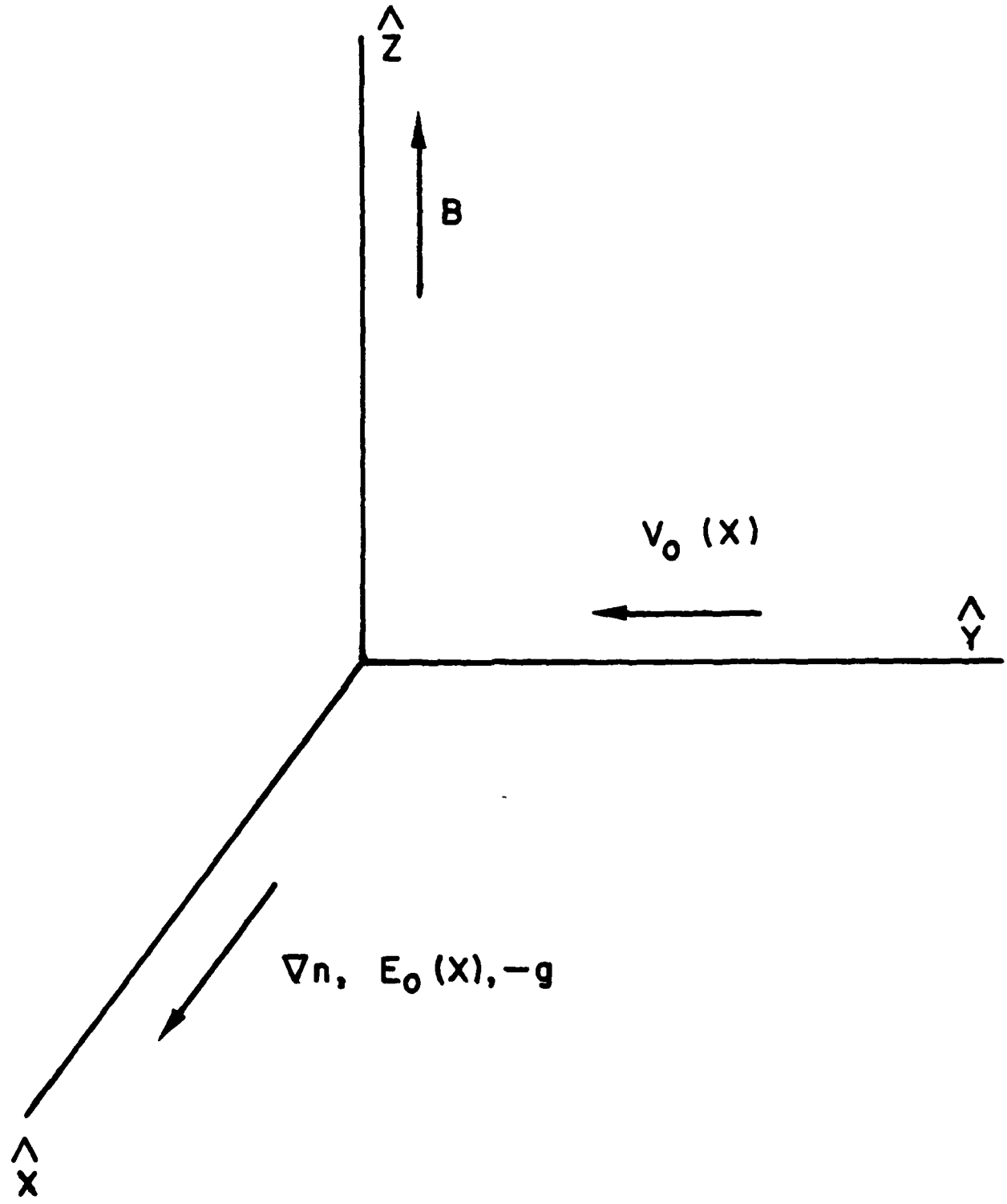

Figure 1. Plasma configuration and slab geometry used in the analysis.

crucial to describe the Kelvin-Helmholtz instability driven by transverse velocity shear (Mikhailovskii, 1974).

Based upon the assumptions discussed above, the fundamental fluid equations used in the analysis are continuity and momentum transfer in the neutral frame of reference:

$$\frac{\partial n_\alpha}{\partial t} + \nabla \cdot (n_\alpha \underline{V}_\alpha) = 0, \tag{1}$$

$$0 = \underline{E} + \frac{1}{c} \underline{V}_e \times \underline{B}, \tag{2}$$

$$m_i\left(\frac{\partial}{\partial t} + \underline{V}_i \cdot \nabla\right) \underline{V}_i = e\underline{E} + \frac{e}{c}\left(\underline{V}_i \times \underline{B}\right) - m_i \nu_{in} \underline{V}_i + m_i \underline{g}. \tag{3}$$

where α denotes species (e for electrons; i for ions).

The equilibrium velocities are, for electrons

$$\underline{V}_{e0}(x) \equiv \underline{V}_0(x) = (c/B)\, \underline{E}_0(x) \times \hat{\underline{z}}\ , \tag{4}$$

and for ions (to order ν_{in}/Ω_i)

$$\underline{V}_{i0}(x) = (c/B)\ \{\ [\underline{E}_0 + (m_i/e)\underline{g}] \times \hat{\underline{z}}\ + (\nu_{in}/\Omega_i)\ [\underline{E}_0 + (m_i/e)\underline{g}] + (1/\Omega_i)\ (\underline{V}_{i0} \cdot \nabla)\ \underline{E}_0\} \tag{5}$$

where $\Omega_i = eB/m_i c$. The electrons simply $\underline{E} \times \underline{B}$ drift, while the ions drift with $\underline{V}_{i0}$, which incorporates the $\underline{E} \times \underline{B}$ drift, and the effects of gravity and the polarization electric field.

We substitue $\underline{E} = -\underline{\nabla}\phi = -\underline{\nabla}\ (\phi_o(x) + \delta\phi)$, $\underline{V}_\alpha = \underline{V}_{\alpha 0}(x) + \delta\underline{V}_\alpha$, $n = n_0(x) + \delta n$ into Eqs. (1) - (3). To obtain the perturbed velocities we do not Fourier analyze the perturbed quantities in the x direction since the

equilibrium quantities vary in that direction; we Fourier analyze only in the y direction. Linearizing Eqs. (2) and (3) and making use of Eqs. (4) and (5), we find the perturbed velocities to be

$$\delta \underline{V}_e = - (c/B) \left[ik_y \, \delta\phi \, \hat{\underline{x}} + \frac{\partial}{\partial x} \delta\phi \, \underline{y}\right], \tag{6}$$

$$\delta \underline{V}_i = \frac{(c/B)}{(1 + V_0'/\Omega_i)} \left[- ik_y \delta\phi + \frac{i\tilde{\omega} - \nu_{in}}{\Omega_i} \frac{\partial}{\partial x} \delta\phi\right] \hat{\underline{x}}$$

$$+ (c/B) \left[\frac{\partial}{\partial x} \delta\phi - \frac{\tilde{\omega} + i\nu_{in}}{\Omega_i} k_y \, \delta\phi\right] \hat{\underline{y}}, \tag{7}$$

where $\tilde{\omega} = \omega - k_y V_0(x)$ and $V_0 = V_{0y} = -(c/B) \, E_{0x}$.

We substitute Eqs. (6) and (7) into Eq. (1), to obtain

$$\frac{\partial}{\partial t} \delta n_e + i \, k_y V_0 \, \delta n_e - i \, \frac{c}{B} \, k_y \, \delta\phi \, n_0' = 0 \tag{8}$$

and

$$\frac{\partial}{\partial t} \delta n_i - \frac{c}{B \, \Omega_i} n_0 \left[(- i\omega + \nu_{in} + k_y V_0) \left(\frac{\partial^2}{\partial x^2} - k_y^2\right) \delta\phi \right.$$

$$\left. + \, i \, k_y \, V_0'' \, \delta\phi + \nu_{in}' \frac{\partial}{\partial x} \delta\phi\right]$$

$$- \frac{c}{B} \, ik_y \, (1 - V_0'/\Omega_i] \, n_0' \, \delta\phi$$

$$- \frac{c}{B \, \Omega_i} (- i \, \omega + \nu_{in} + i \, k_y V_0) \, n_0' \frac{\partial}{\partial x} \delta\phi \tag{9}$$

$$+ (g/\Omega_i - V_0) \, ik_y \delta n_i + (\nu_{in}/\Omega_i) \, (g/\Omega_i - V_0) \frac{\partial}{\partial x} \delta n_i$$

$$+ \frac{\delta n_i}{\Omega_i} \left[(g/\Omega_i - V_0) \, \nu_{in}' + \nu_{in} V_0' \right] = 0$$

where we have ignored terms of order $O(\omega/\Omega_i)$ but have retained terms proportional to ω/ν_{in} and the derivatives of the equilibrium quantities with respect to x (indicated by the primes). We now subtract the electron continuity equation, Eq. (8), from the ion continuity equation, Eq. (9), and impose quasineutrality ($\delta n_e = \delta n_i$). We use Eq. (8) to eliminate δn_i and obtain the mode structure equation

$$\frac{\partial^2}{\partial x^2}\,\delta\phi + p\,\frac{\partial}{\partial x}\,\delta\phi + q\,\delta\phi = 0, \tag{10}$$

where

$$p = \frac{n_0'}{n_0} + \frac{i\nu_{in}}{(\tilde{\omega} + i\nu_{in})}\left(\frac{\nu_{in}'}{\nu_{in}} - \frac{(n_0'/n_0)k_y V_0}{\tilde{\omega}}\right) \tag{11}$$

$$q = -k_y^2 + \frac{k_y(V_0'(n_0'/n_0) + V_0'')}{(\tilde{\omega} + i\nu_{in})} + \frac{k_y^2\, g\,(n_0'/n_0)}{\tilde{\omega}(\tilde{\omega} + i\nu_{in})}$$

$$- \frac{i\nu_{in}\, k_y V_0}{\tilde{\omega}(\tilde{\omega} + i\nu_{in})}\left[\frac{\omega}{\tilde{\omega}}(n_0'/n_0)(V_0'/V_0) + (n_0''/n_0) + (\nu_{in}'/\nu_{in})(n_0'/n_0)\right] \tag{12}$$

Note that the solution of Eq. (10) allows for wavepacket formation instead of plane waves. The properties of the wavepacket are governed by the coefficients p and q. From the expression for q we see that the second term involves the free energy associated with the inhomogeneous plasma flow giving rise to Kelvin-Helmholtz instability. The third term has the gravity and the inverted density gradient leading to Rayleigh-Taylor instability. The last term becomes important in the moderately collisional domain.

Now we define the following dimensionless parameters in order to cast Eq. (10) into a dimensionless form

$$\hat{\omega} = \omega/(g/L)^{1/2},\ \hat{\nu} = \nu_{in}/(g/L)^{1/2},\ \hat{V}_0 = V_0/(gL)^{1/2},\ \text{and}\ \hat{k} = k_y L \tag{13}$$

where L is the characteristic inhomogeneity scale length. We also normalize x with L and define a new independent variable $\chi \equiv x/L$. With these definitions, Eqs. (10)-(12) become

$$\frac{\partial^2}{\partial\chi^2}\,\delta\phi + p\,\frac{\partial}{\partial\chi}\,\delta\phi + q\,\delta\phi = 0, \tag{14}$$

$$p = (n_0/n_0') + i\,\frac{\hat{\nu}}{\hat{\omega}_2}\left[\frac{\hat{\nu}'}{\hat{\nu}} - \frac{(n_0'/n_0)\,\hat{k}\,\hat{V}_0}{\hat{\omega}_1}\right], \tag{15}$$

$$q = -\hat{k}^2 + \hat{k}\left\{\frac{[\hat{V}_0'\,(n_0'/n_0) + \hat{V}_0'']}{\hat{\omega}_2} + \frac{\hat{k}^2\,(n_0'/n_0)}{\hat{\omega}_1\,\hat{\omega}_2}\right\}$$

$$- \frac{i\,\hat{\nu}}{\hat{\omega}_1\,\hat{\omega}_2}\,\hat{k}\,\hat{V}_0\left[(\hat{V}_0'/\hat{V}_0)(n_0'/n_0)(\hat{\omega}/\omega) + (n_0''/n_0) + (n_0'/n_0)(\hat{\nu}'/\hat{\nu})\right] \tag{16}$$

where $\hat{\omega}_1 = \hat{\omega} - \hat{k}\,\hat{V}_0(\chi)$ and $\hat{\omega}_2 = \hat{\omega}_1 + i\,\hat{\nu}$.

We use the transformation

$$\delta\phi(\chi) = \psi(\chi)\ e^{-\int^{\chi} p(\eta)\,d\eta} \tag{17}$$

to write the Eq. (14) as

$$\psi'' + Q(\chi)\,\psi = 0, \tag{18}$$

where

$$Q(\chi) = q(\chi) - p'(\chi)/2 - p(\chi)^{2/4}. \tag{19}$$

In solving the eigenvalue problem, we use WKB boundary conditions on ψ:

$$\psi \to (1/Q^{1/4}) \exp(-\int_0^{\chi} Q(\eta)\, d\eta\,) \quad \text{as } \chi \to \pm\infty\ . \tag{20}$$

We refer to $Q(\chi)$ as the potential function and we give the plots of $Q(\chi)$ and ψ when we solve Eq. (18) numerically in the next section.

Equations similar to Eq. (18) have been obtained by several authors studying the stability of stratified shear layers in neutral fluids (Drazin, 1958). However, usually a Rayleigh-Taylor stable density profile was chosen, mainly to examine the influence of inertia on the velocity shear induced mixing phenomenon. This situation differs slightly from the one considered in this paper, since we study a situation where inverted density gradients and velocity shear both are sources of free energy. The collisionless case can be compared with the neutral fluid case, and when we set $\hat{\nu} = 0$, in Eqs. (14)-(16) we regain the mode structure equation obtained by Drazin (1958). Drazin (1958) considers a weakly inhomogeneous plasma, i.e., by setting n_0'/n_0 to zero everywhere except in the driving term containing the gravity, and obtains a simple equation

$$\psi'' + \left[- \hat{k}^2 + \frac{R}{(\alpha - V_0)^2} + \frac{V_0''}{(\alpha - V_0)} \right] \psi = 0 \tag{21}$$

where

$$R \equiv \frac{(g/L)}{(\overline{V}_0/L)^2} \tag{22}$$

and $\alpha = \omega/k_y$. For this weakly inhomogeneous case, the analysis shows that a neutral stability boundary (where the real and the imaginary parts of c are zero) can be obtained as

$$R = \hat{k}^2(1 - \hat{k}^2). \tag{23}$$

This implies that for $R < 1/4$ the system is stable. Hamieri (1979) considered a more general case applicable to a Tormac machine and arrived at a less stringent condition. A theoretical analysis in the collisionless and collisional cases will be presented in a future paper.

III. Analysis and Results

The generalized mode structure equation [Eq. (14)] can be better understood by first considering two limiting cases: (A) the collisionless and collisional Rayleigh-Taylor instability without velocity shear, and (B) the Kelvin-Helmholtz instability with no collisions or gravity.

A. Rayleigh-Taylor Instability

Setting $V_0 = 0$ in Eq. (14) we obtain

$$\psi'' + (n_0'/n_0)\,\psi' - \hat{k}^2\left[1 - \frac{n_0'/n_0}{\hat{\omega}\,(\hat{\omega} + i\hat{\nu})}\right]\psi = 0 \tag{24}$$

Eq. (24) can be solved in the local approximation,

$$\psi(x) \propto \exp(ik_x x);\ k_y^2 L^2 >> k_x^2 L^2 >> 1 \tag{25}$$

and we obtain the well known dispersion relation (Haerendel, 1974; Hudson and Kennel, 1975)

$$\omega^2 + i\nu_{in}\omega + g/L_n = 0 \tag{26}$$

which has the solution

$$\omega = -\frac{i\nu_{in}}{2}\left[1 \pm \left(1 - 4g/L_n\nu_{in}^2\right)\right]^{1/2}, \tag{27}$$

where $L_n^{-1} = \frac{1}{n_0}\frac{\partial n_0}{\partial x}$. Instability can occur when $g/L_n < 0$. The collisionless and collisional solutions are, respectively,

$$\omega = \pm (g/L_n)^{1/2} \qquad \nu_{in} << |2(g/L_n)^{1/2}|, \tag{28}$$

$$\omega = -i\,(g/L_n)/\nu_{in} \qquad \nu_{in} >> |2(g/L_n)^{1/2}|. \tag{29}$$

We now solve Eq. (24) numerically for a density profile

$$n_0 = \bar{n}_0 \exp(-\frac{\chi^2}{2}) + \Delta n. \tag{30}$$

The results are shown in Fig. 2, which is a plot of normalized growth rate, $\hat{\gamma} = \gamma/(g/L)^{1/2}$, vs normalized wave numbers, $\hat{k} = k_y L$. Curve A is for the collisionless Rayleigh-Taylor instability and curve B is for the collisional Rayleigh-Taylor instability with $\hat{\nu} = 0.5$. We use $\Delta n/n_0 = 0.01$ for both cases. As expected, the growth rate maximizes in the regime $\hat{k} >> 1$ and the maximum growth rate agrees well with the growth rate predicted by local theory [Eq. (27)] with the growth rate evaluated at the maximum density gradient. The potential function ($Q(\chi)$ given by Eq. (19)) and the wave function ($\psi(\chi)$), corresponding to $\hat{k} = 1.0$ are shown in Figs. 3 and 4, respectively. We note that for $\Delta n/n_0 = 0.01$, n_0'/n_0 has a maximum at $\chi = -2.4$and a potential well [$-Q(x)$ is a minimum] is formed around this point as can be seen from Fig. 3. We see from Fig. 4 that the wave function also localizes at $\chi = -2.4$. The negative sign implies that the Rayleigh-Taylor instability is active where the density gradient opposes the gravity. We note that the wave function spreads out into the positive region of the x-axis, where the Rayleigh-Taylor instability is locally stable (gravity acts in the same direction as the density gradient).

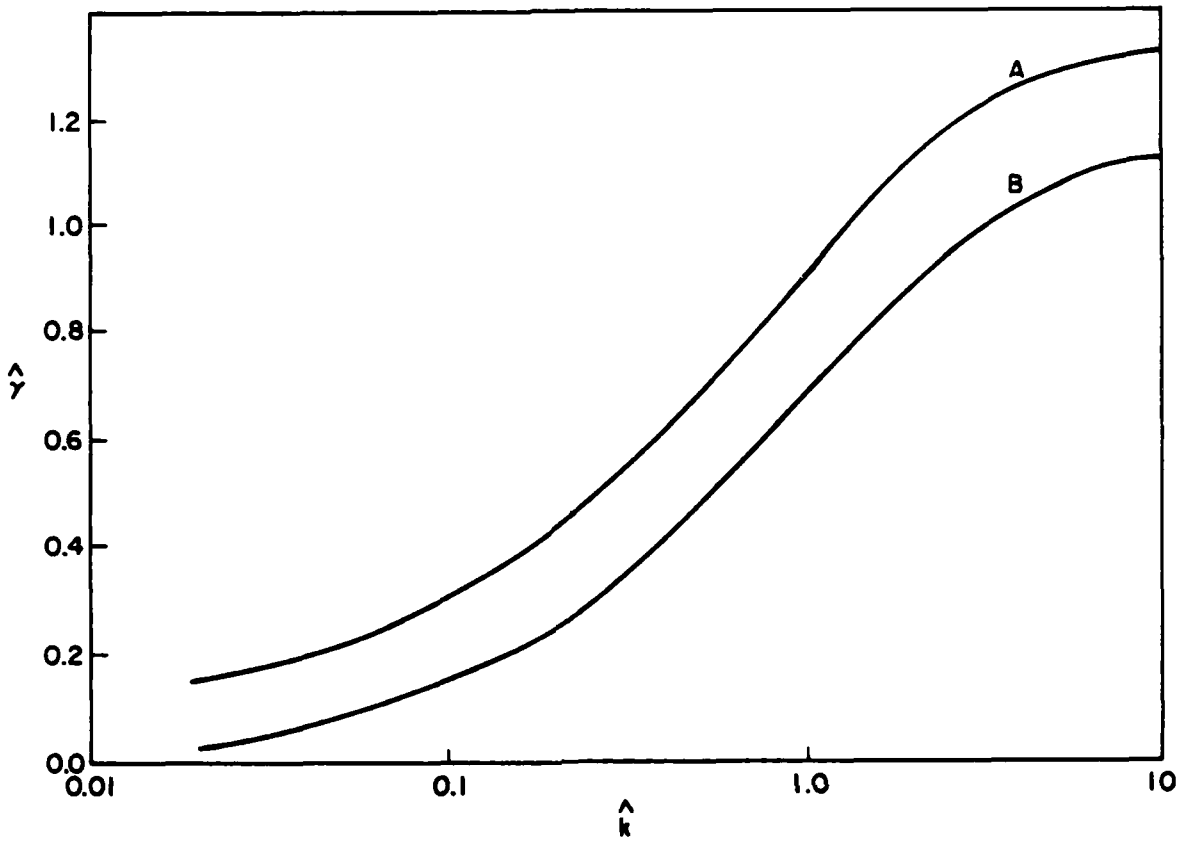

Figure 2. Normalized growth rate $\hat{\gamma} \equiv \gamma/\sqrt{g/L}$ vs $\hat{k} \equiv k_y L$ for the Rayleigh-Taylor instability. Curve A represents the collisionless mode ($\hat{\nu} = 0$); curve B represents the collisional mode ($\hat{\nu} = 0.5$), where $\hat{\nu} = \nu/\sqrt{g/L}$. The density profile used is a Gaussian-like profile $n_0 e^{-x^2/2L^2} + \Delta n$, with $\Delta n/n_0 = 0.01$.

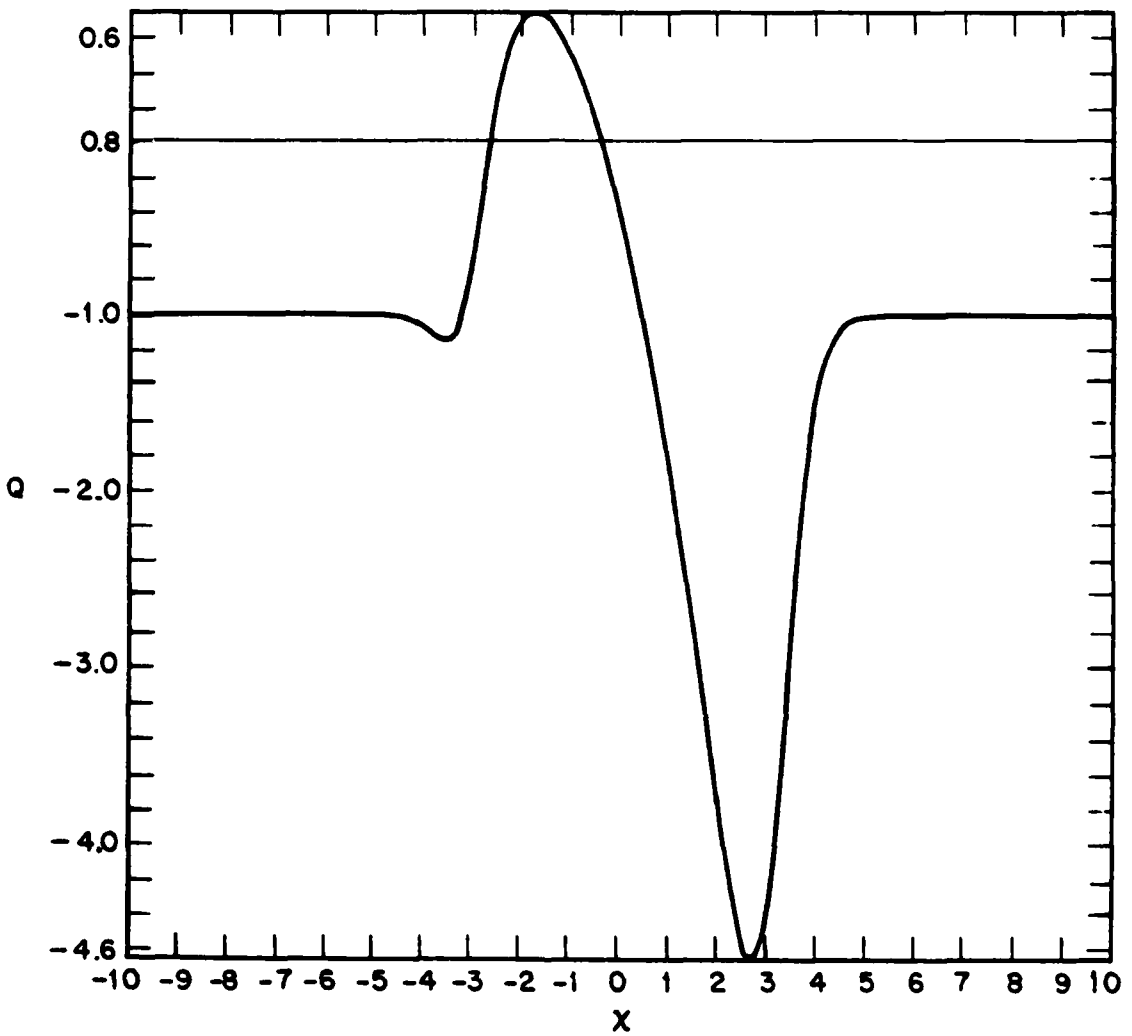

Figure 3. Plot of potential term, $Q(\chi)$, as a function of χ for the collisional case and density profile used in Fig. 2.

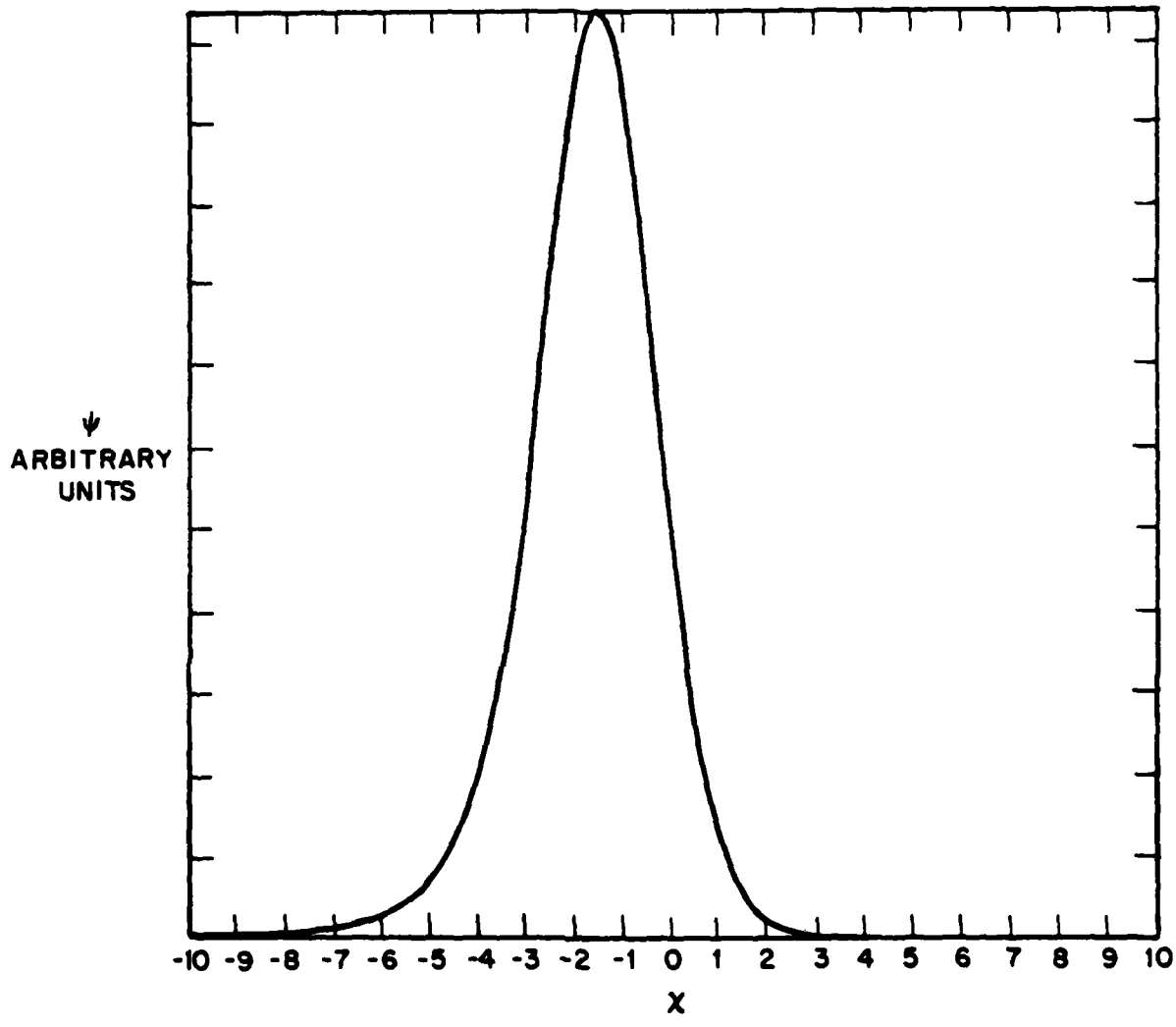

Figure 4. Plot of the wavefunction for $\hat{\omega}_r = 0$, $\hat{\gamma} = .693$, $\hat{k} = 1.0$, and for the collisional case and density profile used in Fig. 2.

B. Kelvin-Helmholtz Instability

We retain the flow velocity $V_0 = V_0(x)$ but consider a collisionless, uniform fluid with no gravity. Eq. (14) becomes

$$\psi'' + [- k_y^2 + \frac{k_y V_0''}{(\omega - k_y V_0)}] \psi = 0, \tag{31}$$

which is well known (Mikhailoviskii, 1974). Rayleigh's theorem (Mikhailovskii, 1974) predicts an instability if the velocity profile has a vanishing second derivative between the boundaries, i.e., $[\partial^2 V_0/\partial x^2]_{x_0} = 0$, where $x_1 < x_0 < x_2$ and x_1 and x_2 are the boundaries.

Equation (31) is solved for an equilibrium velocity profile

$$\underline{V}_0 = \overline{V}_0 \tanh(x/L)\, \hat{y} \tag{32}$$

and the results are shown in Fig. 5 (curve A) in which we plot $\gamma/(V_o/L)$ versus $k_y L$. The instability is purely growing and is bounded between $k_y L = 0$ and 1 with a maximum growth rate of $\gamma \sim 0.18\ (V_o/L)$ at $k_y L \approx 0.45$ (Michalke, 1964).

When a density gradient is included, we arrive at the following equation

$$\psi'' + (n_0'/n_0)\, \psi' + [\, - k_y^2 \, + \frac{[V_0'' + V_0' (n_0'/n_0)]}{(\omega_0 - k_y V_0)}\,]\, \psi = 0. \tag{33}$$

Using the same pocedure as outlined following Eq. (31), we can show that for instabilty the density and velocity profiles should be such that $[\frac{1}{n_0} \frac{\partial}{\partial x} (n_0 V_0')]_{x_0} = 0$ where x_0 is any point within the boundaries. It is interesting to note from Eq. (33) that no instability exists if the density and velocity profiles are such that $V_0''/V_0' = -n_0'/n_0$. Equation (33) is

solved numerically for the velocity profile given in Eq. (32) (in this example we have set the density and shear scale lengths to be equal). The properties of this mode are shown in curve B of Fig. 5 for an exponentially decreasing density profile. Two features are to be noted here: (1) that the density gradient has a stabilizing influence which reduces the maximum growth rate from $\gamma = 0.18\ (V_0/L)$ to $\gamma = 0.074\ (V_0/L)$, and (2) that the instability exists in the region $0.1 < k_y L < 0.9$ shifting the wave number at which the growth rate maximizes from $k_y L = 0.45$ to $k_y L = 0.55$.

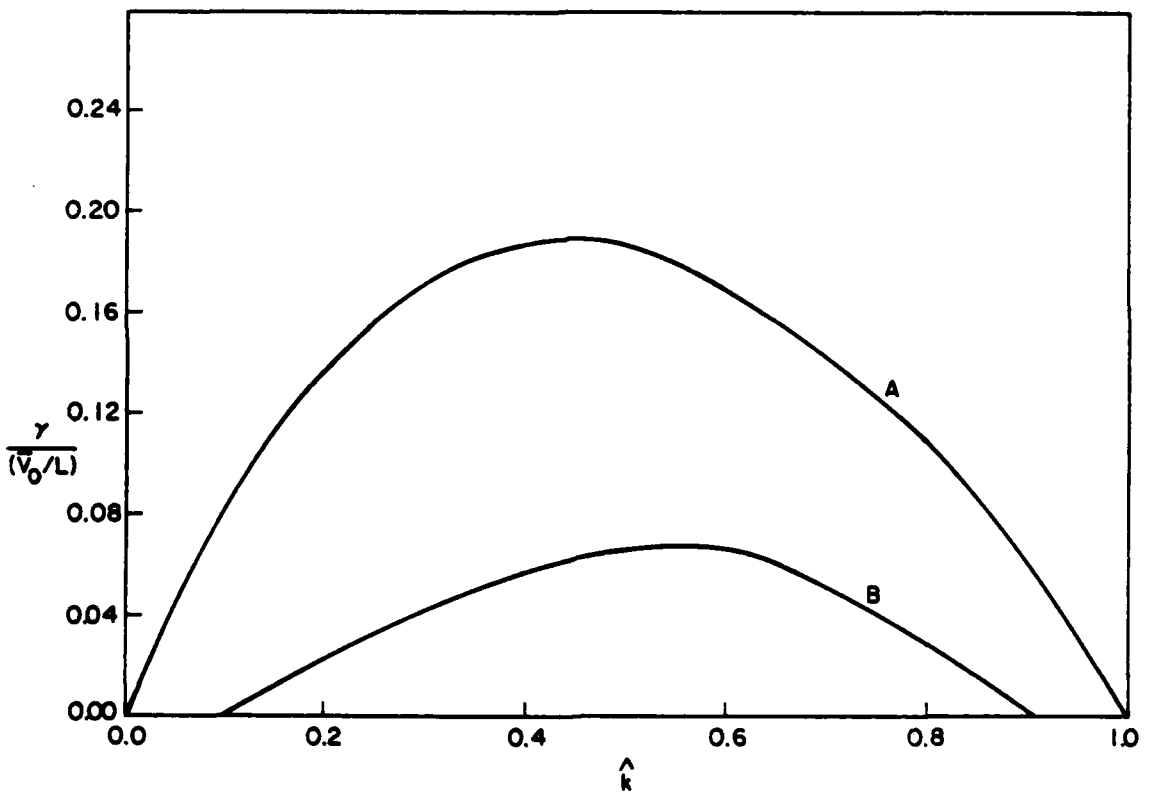

Figure 5. Growth rate $\gamma/(\bar{V}_0/L)$ vs $\hat{k} \equiv k_y L$ for the Kelvin-Helmholtz mode. Curve A represents the case $\hat{\nu} = 0$, $\nabla n = 0$; Curve B represents the case $\hat{\nu} = 0$, and $n_0 = \bar{n}_0 \exp(-x/L)$.

IV. Generalized Rayleigh-Taylor Instability

In the previous section we considered the limiting cases where an inverted density gradient in the presence of gravity and a velocity shear individually give rise to different instabilities. We now consider the general problem where both free energy sources jointly give rise to a generalized Rayleigh-Taylor instability (Hamieri, 1979; Vinas, 1980).

We consider two different cases: (A) a self-consistent equilibrium, and (B) a general equilibrium based on the experimental observations.

A. Self-consistent Equilibrium

We choose the following density profile

$$n_0(x) = \bar{n}_0 \, (1 + \varepsilon \tanh(x/L))/(1-\varepsilon), \tag{34}$$

and the following velocity profile

$$V_0(x) = \bar{V}_0(\bar{n}_0/n_0(x)) \tag{35}$$

such that

$$\hat{V}_0 = \frac{\bar{V}_0}{(gL)^{1/2}} \frac{\bar{n}_0}{n_0(x)} \equiv \hat{s} \frac{\bar{n}_0}{n_0(x)} ,$$

where we have defined a dimensionless parameter $\hat{s} \equiv \bar{V}_0 /(gL)^{1/2}$. Note that the zeroth order continuity equation is satisfied by these profiles for ν_{in} constant, i.e.,

$$\frac{\partial}{\partial x} [(n_0(x) \, V_{i0x}(x)] = 0. \tag{36}$$

which implies

$$n_0(x)\ E_0(x) = \text{constant}$$

or using the definition of V_0 from Eq. (4),

$$n_0(x)\ V_0(x) = \text{constant}.$$

We solve Eq. (14) numerically using these profiles and present the results below.

In Fig. 6 we plot the normalized growth rate $\hat{\gamma}$ versus $\hat{k}$ for the collisionless and collisional cases. The solid lines represent the collisionless case ($\hat{\nu} = 0$) and the dashed lines represent the collisional case ($\hat{\nu} = 0.5$). We set $\varepsilon = 0.8$ in the density profile. Several points are to be noted in this figure. First, we note that in a shear-free, collisionless Rayleigh-Taylor plasma the growth rate asymptotes to the local growth rate evaluated at the peak density gradient, (solid line), i.e.,

$$\gamma(\hat{k} >> 1) = [g(n_0'/n_0)]^{1/2}_{\chi = \bar{\chi}}. \tag{37}$$

For the density profile given in Eq. (36) n_0'/n_0 maximizes at $\bar{\chi}$ obtained from

$$\tanh\chi = [-1 \pm (1 - \varepsilon^2)^{1/2}]/\varepsilon. \tag{38}$$

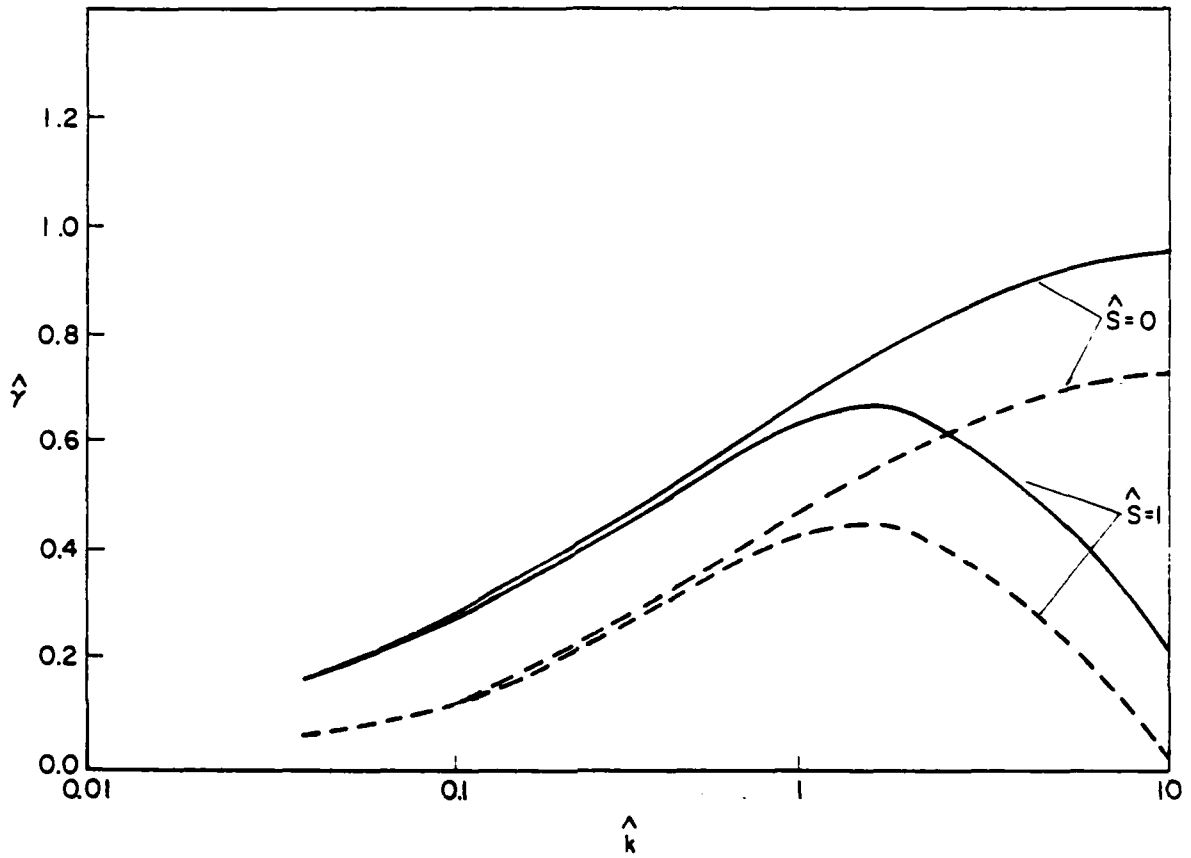

Figure 6. Growth rate $\hat{\gamma}$ vs $\hat{k}$ for the generalized Rayleigh-Taylor instability. Solid lines represent the collisionless case ($\hat{\nu}$ = 0.0, $\hat{s}$ = 0.0, and 1.0); dashed lines represent the collisional case ($\hat{\nu}$ = 0.5, $\hat{s}$ = 0.0, and 1.0). The profiles used are the self-consistent profiles, Eqs. (34) and (35).

For $\varepsilon = 0.8$ Eq. (38) yields $\bar{\chi} = -0.55$ and using this in Eq. (37) we find the local growth rate to be $\hat{\gamma} = 1.0$. This agrees with the growth rate for large $\hat{k}$ (see Fig. 6, solid line). Second, we find that ion-neutral collisions have a stabilizing influence as seen from the dashed line, which represents the growth rate curve for $\hat{\nu} = 0.5$ and $\hat{s} = 0$. Third, in a collisionless Rayleigh-Taylor unstable plasma, for $\hat{s} = 1.0$ (shear frequency, $\bar{V}_0/L$, equal to $\sqrt{g/L}$) velocity shear stabilizes the short wavelength modes (solid line; $\hat{s} = 1.0$); the cut-off mode number, where the growth rate becomes zero, is $\hat{k}_c \sim 11.0$. As a result the growth rate maximizes at $\hat{k} \sim 1.5$ and has a maximum value $\hat{\gamma}_m = 0.675$. Fourth, in a collisional plasma also, with $\hat{\nu} \sim 0.5$ the short wavelength modes are completely stabilized (dashed line; $\hat{s} = 1.0$). The cut-off mode number in this case is, $\hat{k}_c \sim 10.0$, which is less than that of the collisionless case. The peak growth rate is also smaller with $\hat{\gamma}_m = 0.45$ occurring at $\hat{k} = 1.5$. We see that the ion-neutral collisions not only reduce the growth rate but also reduce the cut-off mode number.

In Fig. 7 we give the plots of the wavefunction for $\hat{s} = 0$, $\hat{k} = 0.5$, $\hat{\nu} = 0.5$, and $\varepsilon = 0.8$. We note that the wavefunction localizes at $\chi_0 = -0.55$ which is the point where the density gradient (n_0'/n_0) has an extremum. The wavefunction localizes at this point because $Q(\chi)$ has a local minimum. We refer to this point (for $\hat{s} = 0$) as the Rayleigh-Taylor localization point. The negative sign indicates that the density gradient has to oppose the gravity for instability.

In Fig. 8 we give the wavefunction for the case $\hat{s} = 1$ with the same ν_{in} and ε as in Fig. 7. The solid and the dotted lines represent the real and imaginary parts of the wavefunction, respectively. We note that when

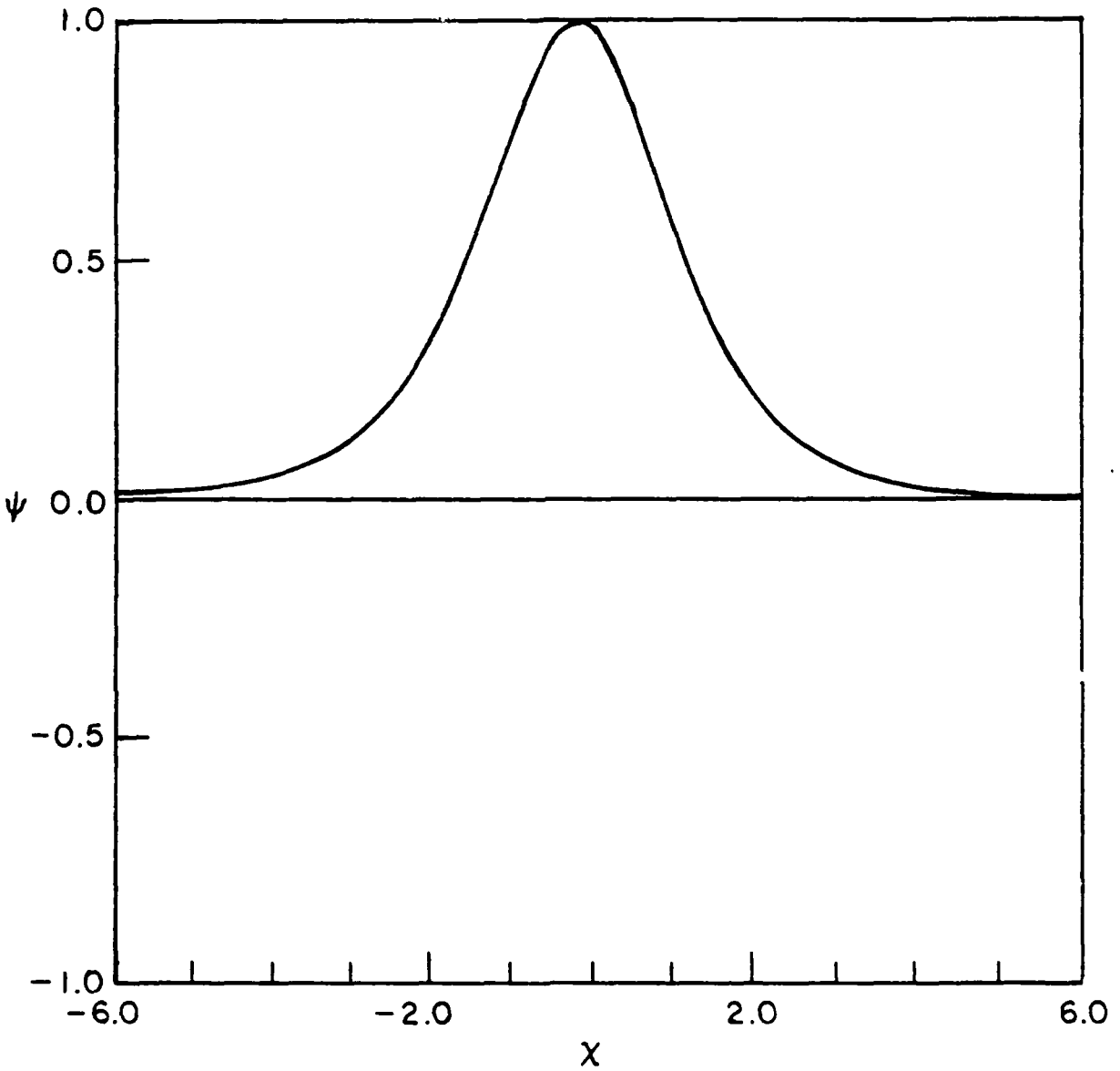

Figure 7. The wave function corresponding to Fig. 6 (solid line; $\hat{s} = 0$) and $\hat{k} = 0.5$.

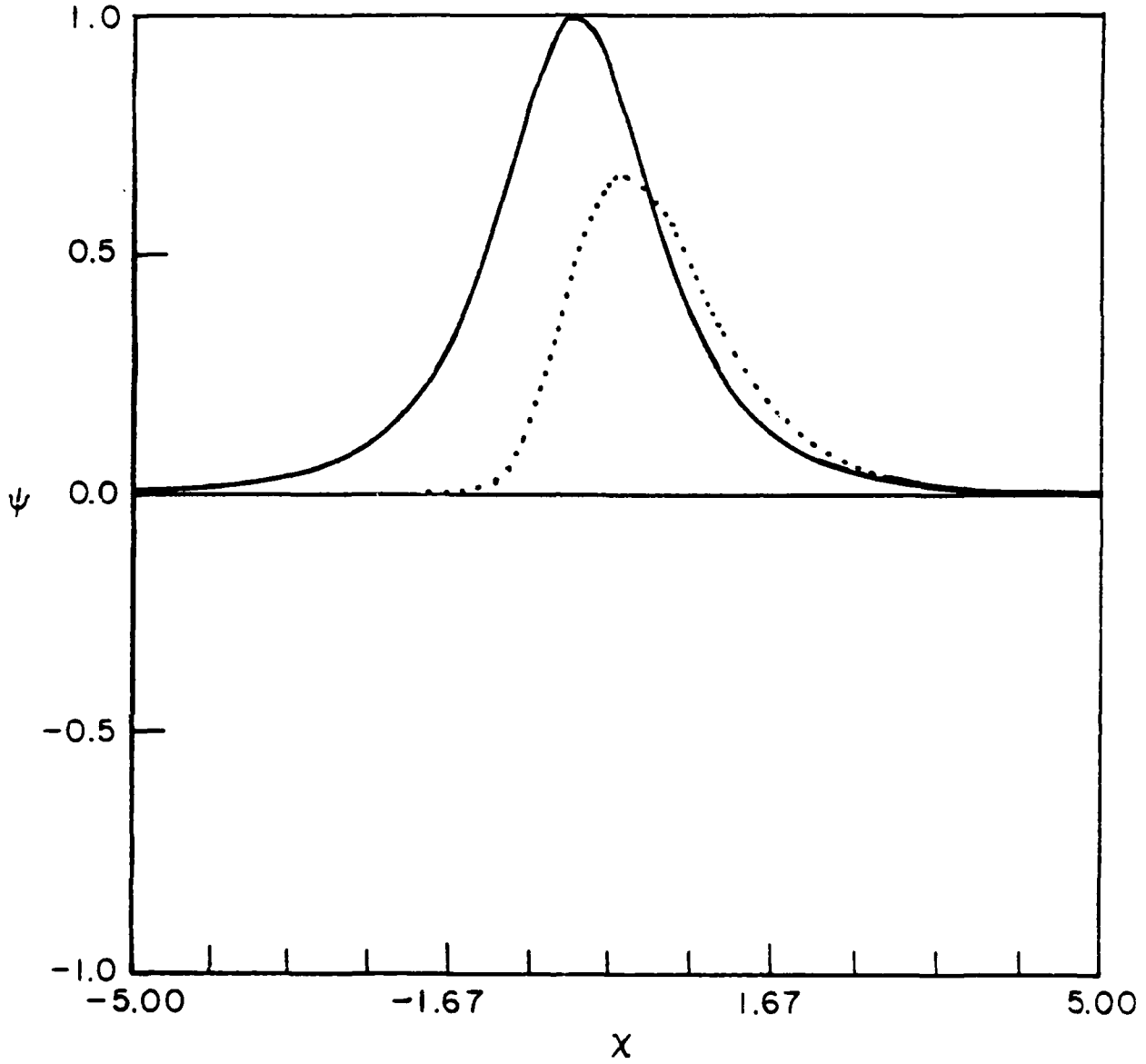

Figure 8. Real and imaginary parts of the wavefunction, corresponding to Fig. 6 (dotted line, $\hat{s} = 1.0$) and $\hat{k} = 0.5$.

the velocity shear is introduced into the problem, the wavefunction picks up an imaginary part. Furthermore, we find that for $\hat{k} \geq 1$, the wavefunction localizes at a point closer to the origin in the velocity shear layer.

In comparing our results with Drazin (1958) we note that since we use a density profile whose density gradient is not a constant, and since we have a Raleigh-Taylor unstable plasma, our threshold condition on R is quite different. This aspect will be dealt with in a future paper.

B. General Equilibrium

Recent experimental observations, made during equatorial spread F (ESF) (Kudeki et al., 1981) and in the high latitude ionospheric F region (Kelley et al., 1978), indicate that ionospheric plasmas usually support inhomogeneous equilibrium plasma flows. In the case of ESF it was found that the flow velocity reverses its direction as a function of altitude ($\hat{x}$, the direction of the density gradient). Furthermore, the velocity reversal point moves up as the spread F develops. This equilibrium situation, where the flow velocity profile is not related to the density profile in a simple manner, is generated by the coupling of the plasma to the neutral atmosphere, for example, by the neutral winds and the inherent shear in the neutral wind velocity or in the case of ESF due to an incomplete coupling caused by background ionospheric Pedersen conductivity away from the equatorial plane (Zalesak et al., 1982). Our earlier numerical results indicate that the inhomogeneity in $\omega - k_y V_0(x)$, and not necessarily the V_0' and V_0'', is primarily responsible for stabilizing the short wavelength interchanger modes (Huba et al., 1983). Therfore, based on the experimental observations (Kudeki et al., 1981; Tsunoda et al., 1981) and our numerical results (Huba et al., 1983), we choose the following density and velocity profiles for a general equilibrium study:

$$n_0(\chi) = \bar{n}_0 \, (1 + \varepsilon \tanh \chi)/(1 - \varepsilon) \tag{39}$$

$$V_0(\chi) = \bar{V}_0 \tanh (\chi - \chi_0) \tag{40}$$

where χ_0 is the velocity reversal point (in the ionospheric case, χ_0 is the point where the westward flow becomes eastward). Using these profiles we solve Eq. (14) numerically. Also, for simplicity, we choose the density gradient scale length and velocity shear scale length to be equal. The numerical results are given below.

First we study the role of χ_0 on stability and determine the optimum χ_0 to be used in later calculations. We set $\hat{\nu} = 0.5$ and $\varepsilon = 0.8$. In Fig. 9 we plot the normalized growth rate $\hat{\gamma}$ versus $\hat{k}$. Curve A shows the nonlocal collisionless Rayleigh-Taylor instability ($\hat{s} = 0$). Curves B, C, and D correspond to $\hat{s} = 1$ for different values of χ_0. Curve B gives the growth rates for $\hat{s} = 1$ and $\chi_0 = -2.0$ which shows a significant reduction in the growth rate. The growth rate maximizes with $\hat{\gamma} = 0.52$ at $\hat{k} \sim 3.0$. However, when χ_0 is set to -0.55 (the Rayleigh-Taylor localization point) the growth rate is sharply reduced, maximizing at $\hat{k} \sim 0.5$ with $\hat{\gamma} = 0.256$ (curve C). For $\chi_0 = 0$ (curve D) there is a significant reduction in the growth rate and a severe reduction of the $\hat{k}$ domain for instability. The instability is bounded between $\hat{k} = 0.5$ and 3.6. Here, the growth rate peaks around $\hat{k} \sim 1.7$. For $\chi_0 = 2.0$ (not shown) the growth rate curve is similar to that of $\chi_0 = -2.0$ (curve C). From this we conclude that the effects of velocity shear are strongest when the velocity reversal point falls in the Rayleigh-Taylor localization region.

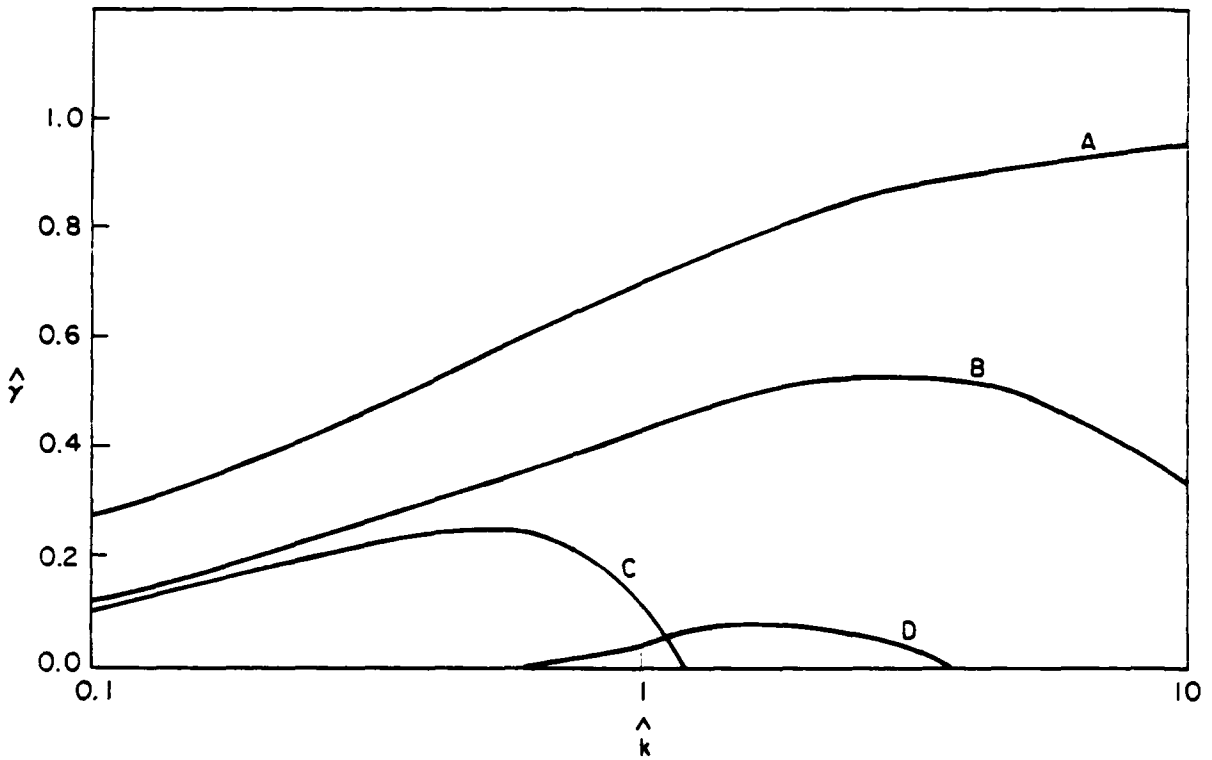

Figure 9. Variation of the dispersion curve, $\hat{\gamma}$ vs $\hat{k}$, for different transition points (χ_0), of the flow velocity profile given by $V = \overline{V}_0 \tanh(\chi - \chi_0)$ for $\chi_0 = -0.5$, -2.0, and 0.0. Parameters used are $\hat{s} = 1$, $\hat{\nu} = 0.5$, $\varepsilon = 0.8$, and for the profiles given in Eqs. (39) and (40). Curve A corresponds to shear-free case ($\hat{s} = 0$) where as curves B, C, and D correspond to $\hat{s} = 1.0$ and $\chi_0 = -2.0$, -0.55, and 0.0 respectively.

In order to throw some light on the variation of the dispersion curves as a function of the velocity shear we plot $\hat{\gamma}$ versus $\hat{k}$ for various values of $\hat{s}$ keeping $\hat{\nu}$, ε, and χ_0 fixed at 0.5, 0.8, and -0.55, respectively, in Fig. 10. This figure shows that the general (non self-consistent) profiles yield results similar to those of the self-consistent profiles (sec. IV.A; see fig. 6). As $\hat{s}$ is increased, $\hat{k}_m$ the mode number at which the growth rate maximizes, moves towards smaller $\hat{k}$ and the growth rate is substantially reduced. For very large shear, $\hat{s} >> 1$, the mode becomes purely Kelvin-Helmholtz like, preferentially exciting a long wavelength mode ($\hat{k} \sim 0.45$) with the cut-off $\hat{k}$ less than 1.0 (to be compared with Fig. 5). This aspect is further illustrated in Fig. 11 where we plot $\hat{\gamma}$ versus $\hat{s}$ for several values of $\hat{k}$. The figure shows that for $\hat{\nu} = 0.5$, modes with $\hat{k} \leq 0.8$ are always unstable. No amount of shear (measured in units of $\hat{s}$) stabilizes these modes due to the onset of the Kelvin-Helmholtz instability for these large $\hat{s}$ and small $\hat{k}$. Furthermore, for the parameters used in the figure, moderate to strong velocity shear stabilizes modes with $\hat{k} > 0.8$. An empirical estimate of the shear that stabilizes the smallest $\hat{k}$ mode can be obtained from the $\hat{k} = 0.8$ curve in Fig. 11, i.e., $\hat{s} = 2.5$ or $\overline{V}_0/L \sim 2.5\sqrt{g/L}$; the figure also shows that the critical shear depends on the wavenumber.

From Fig. 10 we see that for $\hat{\nu} = 0.5$, the mode with $\hat{k} = 0.45$ is the fastest growing mode for large $\hat{s}$. It is interesting to study the behavior of this mode as a function of $\hat{s}$. In Fig. 12 we plot $\hat{\gamma}$ (for $\hat{k} = 0.45$) versus $\hat{s}$. Curves A and B represent the collisionless ($\hat{\nu} = 0$) and collisional ($\hat{\nu} = 0.5$) cases respectively. Note that for $\hat{s} = 0$, $\hat{\gamma}$ is purely Rayleigh-Taylor-like; but as $\hat{s}$ increases, $\hat{\gamma}$ initially decreases, which shows that velocity shear is reducing the growth rate of the Rayleigh-Taylor instability. Beyond $\hat{s} > 1$ the velocity shear dominates and the Kelvin-

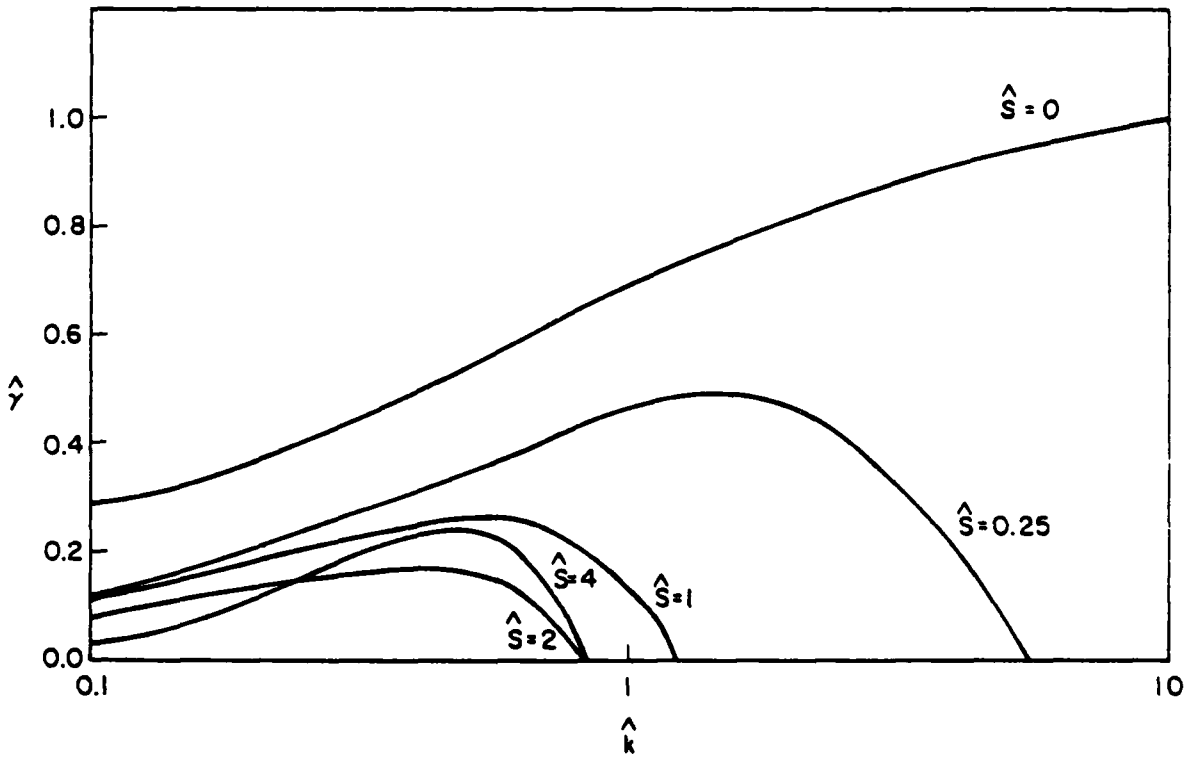

Figure 10. Study of the growth rate as a function of the mode number in the collisional domain $\hat{\gamma}$ vs $\hat{k}$ and for $\hat{s}$ = 0, 0.25, 1.0, 2.0, and 4.0. We have used $\chi_0 = -0.55$, $\hat{\nu} = 0.5$, and $\varepsilon = 0.8$.

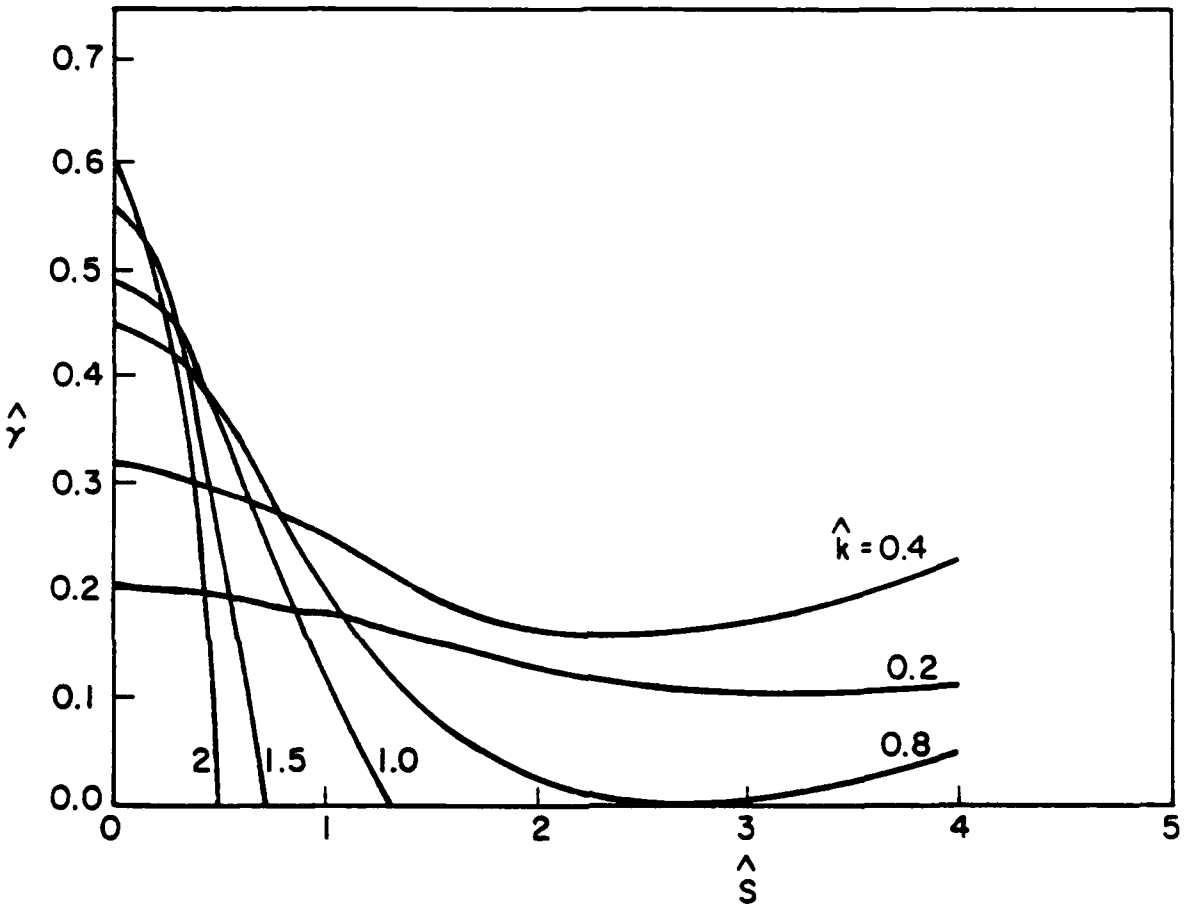

Figure 11. Study of growth rate $\hat{\gamma}$ as a function of $\hat{s}$ for $\hat{k}$ = 0.4 thru 2.0. The parameters used are ε = 0.8, $\hat{\nu}$ = 0.5, and χ_0 = -0.55.

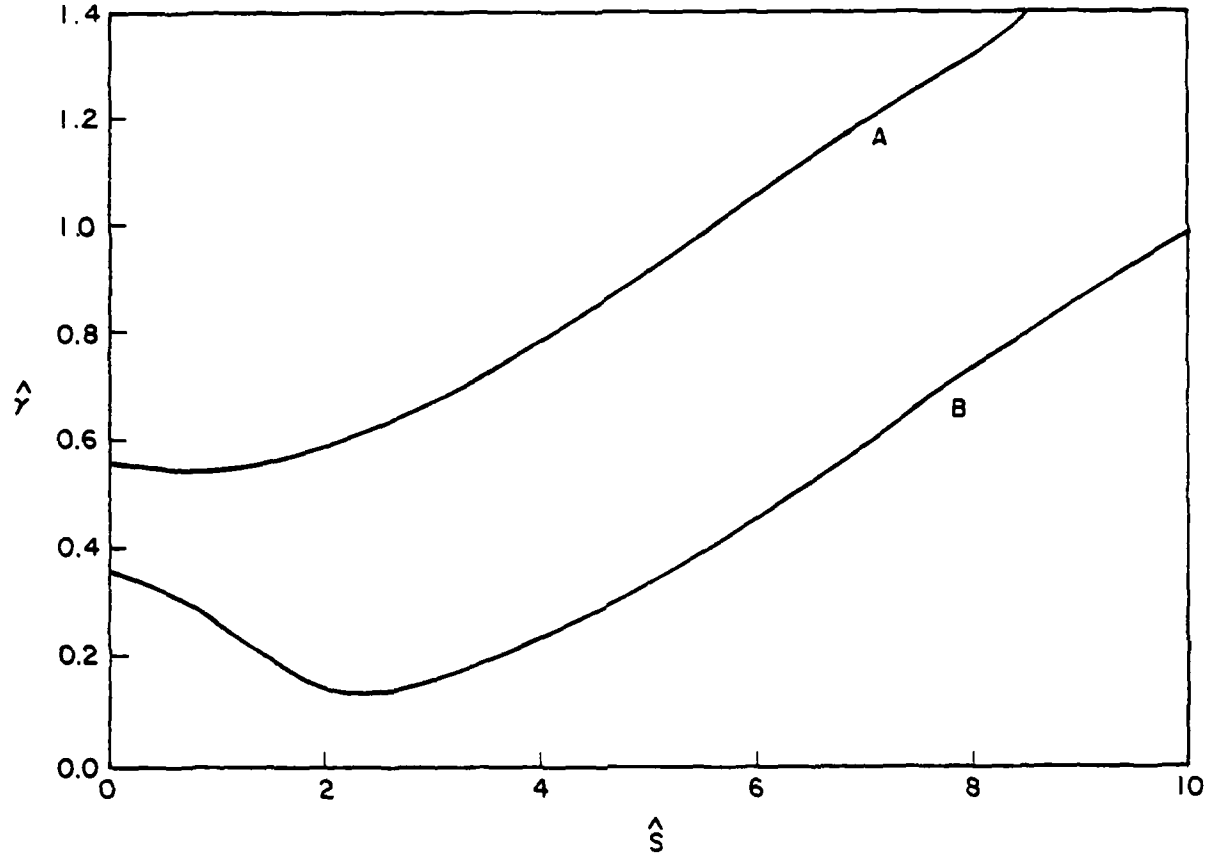

Figure 12. Study of $\hat{\gamma}$ versus $\hat{s}$, for $\hat{k}$ = 0.45 where the Kelvin-Helmholtz instability has maximum growth rate. Curves A and B refer to $\hat{\nu}$ = 0.0 and 0.5 respectively.

Helmholtz mode sets in. We note that $\hat{\gamma}$ increases linearly with $\hat{s}$ for large $\hat{s}$ since it is normalized to $\sqrt{g/L}$ and not $\overline{V}_0/L$. For the collisional case we see that the velocity shear has a stronger influence over a broader domain in $\hat{s}$ and the Kelvin-helmoholtz type instability sets in for larger ($\hat{s} > 2.5$).

We see from Fig. 10 that the cut-off mode numbers and the mode numbers where the growth rate maximizes vary significantly as a function of velocity shear. In order to show the values they asymptote to for large velocity shear, we plot the cut off mode numbers $\hat{k}_c$ (curves A), and the mode numbers of the fastest growing modes, $\hat{k}_m$ (curves B) as a function of $\hat{s}$ in Fig. 13. We use $\chi_0 = -0.55$, $\varepsilon = 0.8$, and $\hat{\nu} = 0$ and 0.5. Solid lines represent the collisionless case ($\hat{\nu} = 0$) and dashed lines represent the collisional case ($\hat{\nu} = 0.5$). From the figure, we see that $\hat{k}_m$, and $\hat{k}_c$ fall sharply as $\hat{s}$ is increased and asymptote to smaller $\hat{k}$ values. For $\hat{\nu} = 0$, (solid lines) $\hat{k}_m$ asymptotes to 0.5 and $\hat{k}_c$ asymptotes to 1.0. Because for large $\hat{s}$ the mode is Kelvin-Helmholtz-like, $\hat{k}_m$ and $\hat{k}_c$,as expected, attain the values shown in Fig. 5. For $\hat{\nu} = 0.5$ (dashed lines) both $\hat{k}_m$ and $\hat{k}_c$ are initially smaller than those for the collisionless case. However, as $\hat{s}$ is increased these maximum and cut-off wavenumbers achieve a minimum value, then rise and again asymptote to similar values as those corresponding to the collisionless case, namely 0.5 and 1.0, respectively.

Finally, in Fig. 14 we show the effects of introducing a spatially dependent collision frequency. In the ionosphere the ion-neutral collision frequency decreases exponentially as a function of the altitude. We use the profile $\hat{\nu} = 0.5\exp(-x/L)$, choosing the scale length to be the same as the density gradient scale length for simplicity. Curve A shows the growth rate curve for constant collision frequency, $\hat{\nu} = 0.5$, and for $\hat{s} = 1.0$, and $\varepsilon = 0.8$. The growth rate maximizes at $\hat{\gamma}_m = 0.256$ around $\hat{k} = 0.55$. Curve B,

with $\hat{\nu} = \hat{\nu}(x)$, shows a drastic reduction in the growth rate. The maximum growth rate ($\hat{\gamma}_m = 0.09$) occurs at $\hat{k} \sim 0.7$. Interestingly, in this case the lowerbound of the instability is shifted. The domain of unstable wave numbers is $0.15 < \hat{k} < 1.2$; whereas, for the constant collision frequency case the domain was $0 < \hat{k} < 1.2$ (the lower bound for curve A is not shown in the figure). Curve C for a weaker shear, namely $\hat{s} = 0.5$, shows that the maximum growth rate is comparable to that of curve A. However, in this case modes with wave numbers $\hat{k} > 3.0$ are completely stabilized.

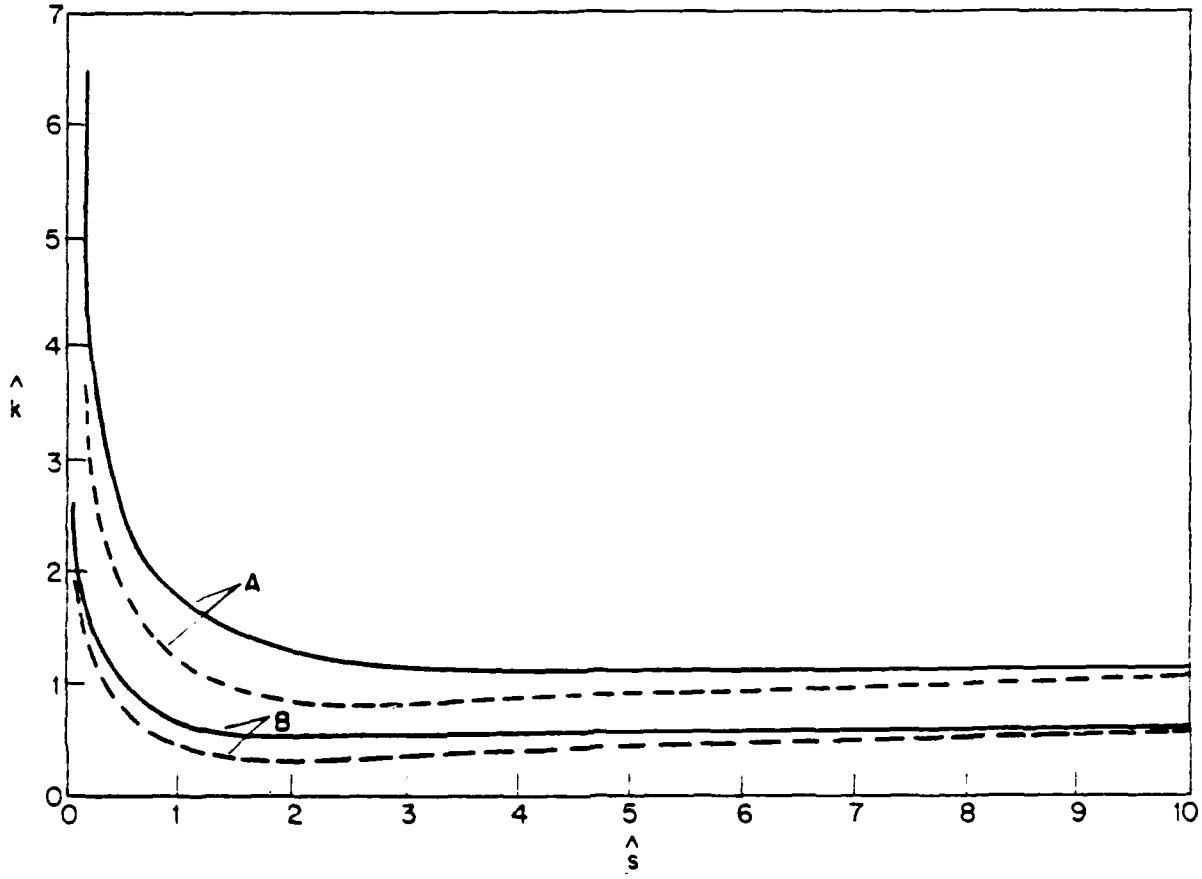

Figure 13. Plots of $\hat{k}_c$ (cut-off mode numbers) and $\hat{k}_m$ (mode numbers where the growth rate maximizes) as a function of $\hat{s}$. The solid and dashed lines correspond to the collisionless and collisional ($\hat{\nu} = 0.5$) cases respectively. Curves A and B refer to $\hat{k}_c$ and $\hat{k}_m$, respectively.

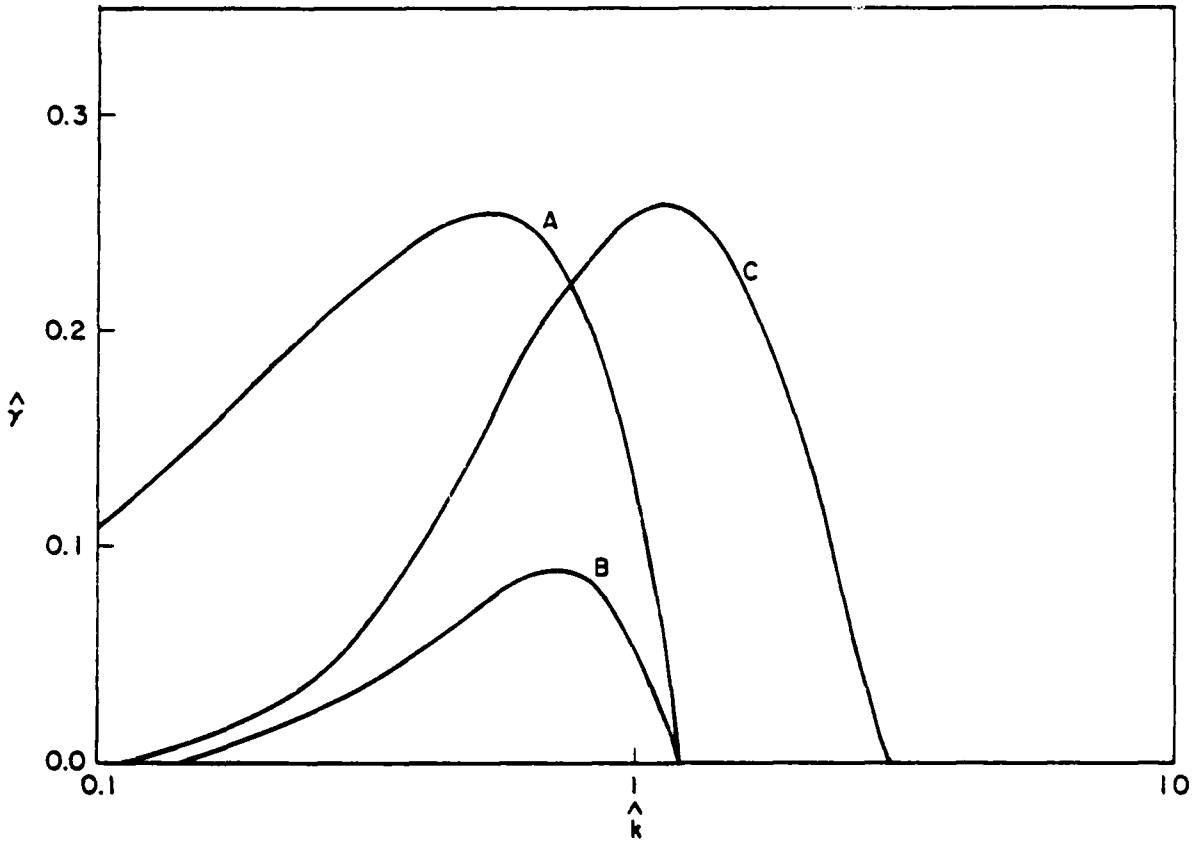

Figure 14. Normalized growth rate versus the normalized wavenumbers for the case of a spatially dependent collision frequency. The density and velocity profiles are given in Eqs. (39) and (40). The parameters used are $\varepsilon = 0.8$, $\chi_0 = -0.55$, and $\hat{\nu} = 0.5$. Curve A refers to constant collision frequency, $\hat{\nu} = 0.5$, and $\hat{s} = 1.0$. Curves B and C refer to $\hat{\nu} = 0.5 \exp(-\chi)$ and for $\hat{s} = 1.0$ and 0.5 respectively.

V. Discussion and Conclusions

We have investigated the influence of velocity shear on the Rayleigh-Taylor instability. The Rayleigh-Taylor instability is driven by gravity and an inverted density gradient. In general this instability is most unstable in the short wavelength domain, $k_y L > 1$, where L is the density inhomogeneity scale length and k_y is perpendicular to the density gradient and the magnetic field. We obtain the well known results that the maximum growth rate is given by $\sqrt{g/L}$ $(g/\nu_{in}L)$ in the collisionless (collisional) domain. On the other hand, a sheared transverse velocity drives the Kelvin-Helmholtz instability in the long wavelength domain, $k_y L < 1$. In the presense of transverse velocity shear, the short wavelength spectrum ($k_y L > 1$) of the Rayleigh-Taylor instability is strongly suppressed or stabilized and the growth rate maximizes in the long wavelength domain ($k_y L < 1$). Thus, velocity shear causes a long wavelength mode to be preferentially excited; whereas in the absense of velocity shear the dominant wave mode usually has a shorter wavelength determined by initial conditions or non-linear processes. This prominant conclusion had been stated in an earlier paper (Guzdar et. al., 1982, 1983). We note that the wavepacket generally localizes in the region where the density gradient opposes the gravity, which in our case also happens to be the shear layer. The wave function falls off rapidly away from the localization region of the Raleigh-Taylor instability, but still has some finite amplitude in the stable region (where $\underline{g}.\nabla n$ is positive). This is due to the global sampling of the entire density profile.

Another interesting feature of the generalized (including velocity shear) Rayleigh-Taylor instability is its crucial dependence on the velocity reversal point. In the absense of velocity shear, the wave function localizes at a point, say χ_w, determined primarily by the background density profile. In the

case of the hyperbolic tangent density profile (Eq. 34), the wave function localizes in the region where the density gradient opposes the gravity. If the velocity reversal point, χ_0 (where the y-component of the equilibrium velocity changes sign), is in the region where the density gradient is parallel to the gravity, the velocity shear has a generally stabilizing influence without the characteristic peak in the growth rate vs wave number curve in the long wavelength domain (Fig. 9). However, when $\chi_w = \chi_0$, velocity shear reduces the growth rate significantly and moves the peak toward longer wavelengths, preferentially exciting longer wavelength modes.

Two possible applications of this theory to ionospheric phenomena have been discussed in a previous paper (Guzdar et al., 1982, 1983). Briefly, the major feature of this theory, viz., preferential excitation of a long wavelength mode, may explain (1) the structuring (1-3 km) of barium releases which are injected across the magnetic field (Linson et al., 1980; Wescott et al., 1980), and (2) the long wavelength (few hundred kms) oscillations of the bottomside F layer during equatorial spread F (Tsunoda and White, 1981; Kelley et al., 1981).

The shaped barium release experiment (Wescott et al., 1980) was conducted at high latitudes in the presence of a pulsating aurora at an altitude of 571 km. Numerical simulations showed that a charge separation induced radial polarization electric field results in an $\underline{E} \times \underline{B}$ velocity shear. This shear layer seems to be located in the region where the density gradient is steepest (Wescott et al., 1980). Our analysis does not strictly apply in the auroral environment. However, the basic instability leading to structuring of the barium cloud is possibly a Rayleigh-Taylor type instability (Pillip, 1971; Fedder, 1980) due to the deceleration of the cloud (Scholer, 1970). So our results in the collisionless domain could be applied to this case. For

example, gradient scale sizes of 500 m - 1 km can lead to irregularity scale sizes of 1.5 - 3 kms with growth rates $\sim 10^{-2}$ sec^{-1}.

Kudeki et al. (1981) have shown, from the observations at Jicamarca using a Radar interferometer technique, that the velocity reversal point moves upward as the spread-F structures evolve. The position of the F-peak was not available at the time of these measurements. However, we conjecture that since the velocity reversal point is at a different location with respect to the F-peak at different times, the velocity shear induced long wavelength modulations of the bottom side F-layer may not be apparent at all times, but may be seen when the velocity reversal point is in the Rayleigh-Taylor localization region (namely, in the bottom side of the F region).

Tsunoda (1983) recently has shown that the background density gradient has a scale length of 25 km when long wavelength fluctuations were observed in the bottom side of the F-layer. No velocity shear measurements, such as the strength of the shear or velocity reversal point, were available. We point out that the measured absense of the velocity shear prior to or immediately after the onset of the wave-like structure is expected because ALTAIR needs the formation of the bubble and spike structures to measure the plasma velocities. Despite the lack of shear data in his paper there is resonable agreement between the data and the theoretical results. However, data on velocity shear, for example by alternate techniques, are crucial to confirm or disprove the theory. The question of short circuiting effects by the E-layer, raised by Tsunoda (1983), needs a closer examination and is not addressed here.

Similar results were obtained by Vinas (1980) in connection with the investigations of the erosion of the plasmapause. He conjectured that strong velocity shear could exist in the plasmapause region and lead to long

wavelength irregularities in competition with the ballooning mode type interchange phenomenon. However, an important difference exists in comparing Vinas' theory with ours, namely, that g/L is positive in his case, meaning that the heavy fluid supports the lighter fluid. We also find similar results in the topside of the equatorial ionosphere, where gravity acts in the same direction as that of the density gradient (a situation similar to Vinas' case) and the collision frequency is very small. These results indicate that in a Rayleigh-Taylor stable plasma the velocity shear could excite Kelvin-Helmholtz type modes. Thus we can conclude that in the absence of equatorial spread F if the flow velocity in the topside ionosphere is sufficiently strongly inhomogeneous, it can induce some large scale irregularities. Figure 5 (curve B) shows that if sufficient velocity shear exists, irregularities of scale sizes of ~ 300 km with weak growth rates (10^{-3} s^{-1}) could possibly exist in the weakly collisional topside of the ionosphere.

In conclusion, we have shown that:

(i) Sheared plasma velocity flows can have pronounced effects on the collisional and collisionless Rayleigh-Taylor instabilities. Sufficiently strong velocity shear preferentially excites a long wavelength mode. This result may explain the long wavelength oscillations of the bottomside F layer during equatorial spread F and the prompt structuring of injected barium clouds (Guzdar et al., 1982; 1983).

(ii) Since the wavefunction localizes in the Rayleigh-Taylor unstable region we expect these long wavelength fluctuations to be seen at the bottomside of the F-layer.

(iii) This phenomenon is most likely to occur when the velocity reversal point is within the Rayleigh-Taylor localization region (where gravity opposes the density gradient).

(iv) The generalized Rayleigh-Taylor instability is qualitatively similar but has quantitatively different properties in the collisional and collisionless domains (see fig. 12). The cut-off mode numbers and maximally growing mode numbers are different in these two cases (see fig. 13).

(v) The properties of the Rayleigh-Taylor instability are similar for self-consistent as well as for general equilibrium density and velocity profiles.

(vi) As the velocity shear is increased, the cut-off mode numbers and the maximally growing mode numbers asymptote to values similar to those of the collisionless Kelvin-Helmholtz instability (see fig. 12).

(vii) A spatially dependent collision frequency alters the results drastically by reducing the growth rate, and by restricting the band of unstable wave numbers to a smaller region (see fig. 14).

ACKNOWLEDGMENTS

This work has been supported by Defence Nuclear Agency and Office of Naval Research. We thank P. Chaturvedi for helpful discussions.

REFERENCES

Bodner, S.E., Rayleigh-Taylor instability and laser-pellet fusion, Phys. Rev. Lett., 33, 761, 1974.

Chandresekhar, S., Hydrodynamic and Hydromagnetic Stabilility, Int. Ser. Monographs on Physics, Clarendon Press, Oxford, 1961, p. 494.

Coppi, B., and M.N. Rosenbluth, Collisional interchange instabilities in shear and ∫dl/B stabilized systems, in Proceedings of the 1965 International Conference on Plasma Physics and controlled Nuclear Fusion Research, Paper CN-21/106, International Atomic Energy Agency, Vienna, 1966.

Coppi, B., J. Filreis, and F. Pegoraro, Analytical representation and physics of ballooning modes, Ann. Phys. (N.Y.) 121, 1, 1979.

Daly, B.J., Numerical study of two fluid Rayleigh-Taylor instability, Phys. Fluids., 10, 297, 1967

Davis, T.N., G.J. Romick, E.M. Wescott, R.A. Jeffries, D.M. Kerr, and H.M. Peek, Observations of the development of striations in large barium ion clouds, Planet. Space Sci., 22, 67, 1974.

Drazin, P.G., The stability of a shear layer in an unbounded heterogeneous inviscid fluid, J. Fluid Mech., 4, 214, 1958.

Emery, M.H., J.H. Gardner, and J.P. Boris, The Rayleigh-Taylor and Kelvin-Helmholtz instabilities in targets accelerated by laser ablation, Phys. Rev. Lett., 48, 677, 1982.

Fedder, J.A., Structuring of collisionless, high velocity ion clouds, Memo Rept. 4307, Nav. Res. Lab., Washington, D.C., September, 1980. AD A089-373

Fejer, B.G.. amd M.C. Kelley, Ionospheric irregularities, Rev. Geophys. Space Phys., 18, 401, 1980.

Guzdar, P.N., P. Satyanarayana, J.D. Huba, and S.L. Ossakow, Influence of velocity shear on Rayleigh-Taylor instability, Geophys. Res. Lett., 9, 547, 1982.

Guzdar, P.N., P. Satyanarayana, J.D. Huba, and S.L. Ossakow, Correction to "Influence of velocity shear on Rayleigh-Taylor instability", Geophys. Res. Lett., 10, 492, 1983.

Haerendel, G. Theory of equatorial spread F, Preprint, Max-Planck Institute for Physik und Astrophysik, Garching, West Germany, 1974.

Hameiri, E., Shear stabilization of the Rayleigh-Taylor modes, Phys. Fluids., 22, 89, 1979.

Harlow, F.H. and J.E. Welch, Numerical study of large-amplitude free-surface motions, Phys. Fluids., 9, 842, 1966.

Huba, J.D., S.L. Ossakow, P. Satyanarayana, and P.N. Guzdar, Linear theory of the $\underline{E} \times \underline{B}$ instability with an inhomogeneous electric field, J. Geophys. Res., 88, 425, 1983.

Hudson, M.K., and C.F. Kennel, Linear theory of equatorial spread F, J. Geophys. Res., 80, 4581, 1975.

Kelley, M.C., M.F. Larsen, C. LaHoz, and J.P. McClure, Gravity wave initiation of equatorial spread F: A case study, J. Geophys. Res., 86,9087, 1981.

Kelvin, Lord, Hydrodynamics and General Dynamics, Cambridge University Press, Cambridge, 1910, p. 69

Kudeki, E., B.G. Fejer, D.T. Farley, and H.M. Ierkic, Interferometer studies of equatorial F region irregularities and drifts, Geophys. Res. Lett., 8, 377, 1981.

Linson, L.M., and J.B. Workman, Formation of striations in ionospheric plasma clouds, J. Geophys. Res., 75, 3211, 1970.

Michalke, A., On the inviscid instability of the hyperbolic-tangent velocity profile, J. Fluid Mech., 19, 543, 1964.

Mikhailovskii, A.B., Theory of Plasma Instabilities: Vol. II, Consultants Bureau, New York, 1974, p. 141.

Ossakow, S.L. Ionospheric irregularities, Rev. Geophys. Space Phys., 17, 521, 1979.

Perkins, F.W. and J.H. Doles III, Velocity shear and the E x B instabilty, J. Geophys. Res., 80, 211, 1975.

Phillipp, W.G., Expansion of an ion cloud in the earth's magnetic field, Planet. Space Sci., 19, 1095, 1971.

Rayleigh, Lord, Theory of Sound, Dover Publications, Inc., New York, 1945.

Rosenberg, N.W., Observations of striation formation in a barium ion cloud, J. Geophys. Res., 76, 6856, 1971.

Scannapieco, A.J. and S.L. Ossakow, Nonlinear equatorial spread F, Geophys. Res. Lett., 3, 451, 1976.

Scannapieco, A.J., S.L. Ossakow, S.R. Goldman, and J.M. Pierre, Plasma cloud late time striation spectra, J. Geophys. Res., 81, 6037, 1976.

Scholer, M., On the motion of artificial ion clouds in the magnetosphere, Planet. Space Sci., 18, 977, 1970.

Simons, D.J., M.B. Pongratz, and S.P. Gary, Prompt striations in ionospheric barium clouds due to a velocity space instability, J. Geophys. Res., 85, 671, 1980.

Taylor, G., The instability of liquid surfaces when accelerated in a direction perpendicular to their planes. I, Pro. of Roy. Soc., (London) Ser. A201, 192, 1950.

Tsunoda, R.T., Time evolution and dynamics of equatorial backscatter plumes, 1. Growth phase, J. Geophys. Res., 86, 139, 1981.

Tsunoda, R.T., ALTAIR radar study of equatorial spread F, SRI International Final Report, DNA 5689F, February, 1981. AD-A104-554

Tsunoda, R.T., R.C. Livingston, and C.L. Rino, Evidence of a velocity shear in bulk plasma motion associated with the post-sunset rise of the equatorial F-layer, Geophys. Res. Lett., 8, 807, 1981.

Tsunoda, R.T., and B.R. White, On the generation and growth of equatorial backscatter plumes-1. Wave structure in the bottomside F layer, J. Geophys. Res.,86, 3610, 1981.

Tsunoda, R.T., On the generation and growth of equatorial backscatter plumes-2. Sructuring of the west walls of upwellings, J. Geophys. Res., 88, 4869, 1983.

Viñas , A.F., Magnetohydrodynamic analysis of the stability of the plasma pause, Ph.D. thesis, MIT, 1980.

Viñas , A.F. and T. Madden, Shear flow balloning instability as a possible mechanism for micropulsations at the plasma pause, J. Geophys. Res., (submitted, 1983).

Wescott, E.M., H.C. Stenback-Nielsen, T.J. Hallinan, C.S. Deehr, G.J. Romick, J.V. Olson, J.G. Roederer, and R. Sydora, A high-altitude barium radial injection experiment, Geophys. Res. Lett., 7, 1037, 1980.

Zabusky, N.J., J.H. Doles III, and F.W. Perkins, Deformation and striation of plasma clouds in the ionosphere, 2. Numerical simulation of a nonlinear two-dimensional model, J. Geophys. Res., 78, 711, 1973.

Zalesak, S.T., and S.L. Ossakow, Nonlinear equatorial spread F: Spatially large bubbles resulting from large horizontal scale initial perturbations, J. Geophys. Res., 85, 2131, 1980.

Zalesak, S.T., S.L. Ossakow, and P.K. Charturvedi, Nonlinear equatorial spread F: The effect of neutral winds and background Pedersen conductivity, J. Geophys. Res, 87, 151, 1982.

DISTRIBUTION LIST

DEPARTMENT OF DEFENSE

ASSISTANT SECRETARY OF DEFENSE
COMM, CMD, CONT 7 INTELL
WASHINGTON, D.C. 20301

DIRECTOR
COMMAND CONTROL TECHNICAL CENTER
PENTAGON RM BE 685
WASHINGTON, D.C. 20301
01CY ATTN C-650
01CY ATTN C-312 R. MASON

DIRECTOR
DEFENSE ADVANCED RSCH PROJ AGENCY
ARCHITECT BUILDING
1400 WILSON BLVD.
ARLINGTON, VA. 22209
01CY ATTN NUCLEAR MONITORING RESEARCH
01CY ATTN STRATEGIC TECH OFFICE

DEFENSE COMMUNICATION ENGINEER CENTER
1860 WIEHLE AVENUE
RESTON, VA. 22090
01CY ATTN CODE R410
01CY ATTN CODE R812

DEFENSE TECHNICAL INFORMATION CENTER
CAMERON STATION
ALEXANDRIA, VA. 22314
02CY

DIRECTOR
DEFENSE NUCLEAR AGENCY
WASHINGTON, D.C. 20305
01CY ATTN STVL
04CY ATTN TITL
01CY ATTN DDST
03CY ATTN RAAE

COMMANDER
FIELD COMMAND
DEFENSE NUCLEAR AGENCY
KIRTLAND, AFB, NM 87115
01CY ATTN FCPR

DIRECTOR
INTERSERVICE NUCLEAR WEAPONS SCHOOL
KIRTLAND AFB, NM 87115
01CY ATTN DOCUMENT CONTROL

JOINT CHIEFS OF STAFF
WASHINGTON, D.C. 20301
01CY ATTN J-3 WWMCCS EVALUATION OFFICE

DIRECTOR
JOINT STRAT TGT PLANNING STAFF
OFFUTT AFB
OMAHA, NB 68113
01CY ATTN JLTW-2
01CY ATTN JPST G. GOETZ

CHIEF
LIVERMORE DIVISION FLD COMMAND DNA
DEPARTMENT OF DEFENSE
LAWRENCE LIVERMORE LABORATORY
P.O. BOX 808
LIVERMORE, CA 94550
01CY ATTN FCPRL

COMMANDANT
NATO SCHOOL (SHAPE)
APO NEW YORK 09172
01CY ATTN U.S. DOCUMENTS OFFICER

UNDER SECY OF DEF FOR RSCH & ENGRG
DEPARTMENT OF DEFENSE
WASHINGTON, D.C. 20301
01CY ATTN STRATEGIC & SPACE SYSTEMS (OS)

WWMCCS SYSTEM ENGINEERING ORG
WASHINGTON, D.C. 20305
01CY ATTN R. CRAWFORD

COMMANDER/DIRECTOR
ATMOSPHERIC SCIENCES LABORATORY
U.S. ARMY ELECTRONICS COMMAND
WHITE SANDS MISSILE RANGE, NM 88002
01CY ATTN DELAS-EO F. NILES

DIRECTOR
BMD ADVANCED TECH CTR
HUNTSVILLE OFFICE
P.O. BOX 1500
HUNTSVILLE, AL 35807
01CY ATTN ATC-T MELVIN T. CAPPS
01CY ATTN ATC-O W. DAVIES
01CY ATTN ATC-R DON RUSS

PROGRAM MANAGER
BMD PROGRAM OFFICE
5001 EISENHOWER AVENUE
ALEXANDRIA, VA 22333
01CY ATTN DACS-BMT J. SHEA

CHIEF C-E- SERVICES DIVISION
U.S. ARMY COMMUNICATIONS CMD
PENTAGON RM 1B269
WASHINGTON, D.C. 20310
01CY ATTN C- E-SERVICES DIVISION

COMMANDER
FRADCOM TECHNICAL SUPPORT ACTIVITY
DEPARTMENT OF THE ARMY
FORT MONMOUTH, N.J. 07703
01CY ATTN DRSEL-NL-RD H. BENNET
01CY ATTN DRSEL-PL-ENV H. BOMKE
01CY ATTN J.E. QUIGLEY

COMMANDER
U.S. ARMY COMM-ELEC ENGRG INSTAL AGY
FT. HUACHUCA, AZ 85613
01CY ATTN CCC-EMEO GEORGE LANE

COMMANDER
U.S. ARMY FOREIGN SCIENCE & TECH CTR
220 7TH STREET, NE
CHARLOTTESVILLE, VA 22901
01CY ATTN DRXST-SD

COMMANDER
U.S. ARMY MATERIAL DEV & READINESS CMD
5001 EISENHOWER AVENUE
ALEXANDRIA, VA 22333
01CY ATTN DRCLDC J.A. BENDER

COMMANDER
U.S. ARMY NUCLEAR AND CHEMICAL AGENCY
7500 BACKLICK ROAD
BLDG 2073
SPRINGFIELD, VA 22150
01CY ATTN LIBRARY

DIRECTOR
U.S. ARMY BALLISTIC RESEARCH LABORATORY
ABERDEEN PROVING GROUND, MD 21005
01CY ATTN TECH LIBRARY EDWARD BAICY

COMMANDER
U.S. ARMY SATCOM AGENCY
FT. MONMOUTH, NJ 07703
01CY ATTN DOCUMENT CONTROL

COMMANDER
U.S. ARMY MISSILE INTELLIGENCE AGENCY
REDSTONE ARSENAL, AL 35809
01CY ATTN JIM GAMBLE

DIRECTOR
U.S. ARMY TRADOC SYSTEMS ANALYSIS ACTIVITY
WHITE SANDS MISSILE RANGE, NM 88002
01CY ATTN ATAA-SA
01CY ATTN TCC/F. PAYAN JR.
01CY ATTN ATTA-TAC LTC J. HESSE

COMMANDER
NAVAL ELECTRONIC SYSTEMS COMMAND
WASHINGTON, D.C. 20360
01CY ATTN NAVALEX 034 T. HUGHES
01CY ATTN PME 117
01CY ATTN PME 117-T
01CY ATTN CODE 5011

COMMANDING OFFICER
NAVAL INTELLIGENCE SUPPORT CTR
4301 SUITLAND ROAD, BLDG. 5
WASHINGTON, D.C. 20390
01CY ATTN MR. DUBBIN STIC 12
01CY ATTN NISC-50
01CY ATTN CODE 5404 J. GALET

COMMANDER
NAVAL OCEAN SYSTEMS CENTER
SAN DIEGO, CA 92152
01CY ATTN J. FERGUSON

NAVAL RESEARCH LABORATORY
WASHINGTON, D.C. 20375
01CY ATTN CODE 4700 S. L. Ossakow
26 CYS IF UNCLASS. 1 CY IF CLASS)
01CY ATTN CODE 4701 I Vitkovitsky
01CY ATTN CODE 4780 J. Huba (100
CYS IF UNCLASS, 1 CY IF CLASS)
01CY ATTN CODE 7500
01CY ATTN CODE 7550
01CY ATTN CODE 7580
01CY ATTN CODE 7551
01CY ATTN CODE 7555
01CY ATTN CODE 4730 E. MCLEAN
01CY ATTN CODE 4108
01CY ATTN CODE 4730 B. RIPIN
20CY ATTN CODE 2628

COMMANDER
NAVAL SEA SYSTEMS COMMAND
WASHINGTON, D.C. 20362
01CY ATTN CAPT R. PITKIN

COMMANDER
NAVAL SPACE SURVEILLANCE SYSTEM
DAHLGREN, VA 22448
01CY ATTN CAPT J.H. BURTON

OFFICER-IN-CHARGE
NAVAL SURFACE WEAPONS CENTER
WHITE OAK, SILVER SPRING, MD 20910
01CY ATTN CODE F31

DIRECTOR
STRATEGIC SYSTEMS PROJECT OFFICE
DEPARTMENT OF THE NAVY
WASHINGTON, D.C. 20376
01CY ATTN NSP-2141
01CY ATTN NSSP-2722 FRED WIMBERLY

COMMANDER
NAVAL SURFACE WEAPONS CENTER
DAHLGREN LABORATORY
DAHLGREN, VA 22448
01CY ATTN CODE DF-14 R. BUTLER

OFFICER OF NAVAL RESEARCH
ARLINGTON, VA 22217
01CY ATTN CODE 465
01CY ATTN CODE 461
01CY ATTN CODE 402
01CY ATTN CODE 420
01CY ATTN CODE 421

COMMANDER
AEROSPACE DEFENSE COMMAND/DC
DEPARTMENT OF THE AIR FORCE
ENT AFB, CO 80912
01CY ATTN DC MR. LONG

COMMANDER
AEROSPACE DEFENSE COMMAND/XPD
DEPARTMENT OF THE AIR FORCE
ENT AFB, CO 80912
01CY ATTN XPDQQ
01CY ATTN XP

AIR FORCE GEOPHYSICS LABORATORY
HANSCOM AFB, MA 01731
01CY ATTN OPR HAROLD GARDNER
01CY ATTN LKB KENNETH S.W. CHAMPION
01CY ATTN OPR ALVA T. STAIR
01CY ATTN PHD JURGEN BUCHAU
01CY ATTN PHD JOHN P. MULLEN

AF WEAPONS LABORATORY
KIRTLAND AFT, NM 87117
01CY ATTN SUL
01CY ATTN CA ARTHUR H. GUENTHER
01CY ATTN NTYCE 1LT. G. KRAJEI

AFTAC
PATRICK AFB, FL 32925
01CY ATTN TF/MAJ WILEY
01CY ATTN TN

AIR FORCE AVIONICS LABORATORY
WRIGHT-PATTERSON AFB, OH 45433
01CY ATTN AAD WADE HUNT
01CY ATTN AAD ALLEN JOHNSON

DEPUTY CHIEF OF STAFF
RESEARCH, DEVELOPMENT, & ACQ
DEPARTMENT OF THE AIR FORCE
WASHINGTON, D.C. 20330
01CY ATTN AFRDQ

HEADQUARTERS
ELECTRONIC SYSTEMS DIVISION
DEPARTMENT OF THE AIR FORCE
HANSCOM AFB, MA 01731
01CY ATTN J. DEAS

HEADQUARTERS
ELECTRONIC SYSTEMS DIVISION/YSEA
DEPARTMENT OF THE AIR FORCE
HANSCOM AFB, MA 01732
01CY ATTN YSEA

HEADQUARTERS
ELECTRONIC SYSTEMS DIVISION/DC
DEPARTMENT OF THE AIR FORCE
HANSCOM AFB, MA 01731
01CY ATTN DCKC MAJ J.C. CLARK

COMMANDER
FOREIGN TECHNOLOGY DIVISION, AFSC
WRIGHT-PATTERSON AFB, OH 45433
01CY ATTN NICD LIBRARY
01CY ATTN ETDP B. BALLARD

COMMANDER
ROME AIR DEVELOPMENT CENTER, AFSC
GRIFFISS AFB, NY 13441
01CY ATTN DOC LIBRARY/TSLD
01CY ATTN OCSE V. COYNE

SAMSO/SZ
POST OFFICE BOX 92960
WORLDWAY POSTAL CENTER
LOS ANGELES, CA 90009
(SPACE DEFENSE SYSTEMS)
01CY ATTN SZJ

STRATEGIC AIR COMMAND/XPFS
OFFUTT AFB, NB 68113
01CY ATTN ADWATE MAJ BRUCE BAUER
01CY ATTN NRT
01CY ATTN DOK CHIEF SCIENTIST

SAMSO/SK
P.O. BOX 92960
WORLDWAY POSTAL CENTER
LOS ANGELES, CA 90009
01CY ATTN SKA (SPACE COMM SYSTEMS)
M. CLAVIN

SAMSO/MN
NORTON AFB, CA 92409
(MINUTEMAN)
01CY ATTN MONL

COMMANDER
ROME AIR DEVELOPMENT CENTER, AFSC
HANSCOM AFB, MA 01731
01CY ATTN EEP A. LORENTZEN

DEPARTMENT OF ENERGY
LIBRARY ROOM G-042
WASHINGTON, D.C. 20545
01CY ATTN DOC CON FOR A. LABOWITZ

DEPARTMENT OF ENERGY
ALBUQUERQUE OPERATIONS OFFICE
P.O. BOX 5400
ALBUQUERQUE, NM 87115
01CY ATTN DOC CON FOR D. SHERWOOD

EG&G, INC.
LOS ALAMOS DIVISION
P.O. BOX 809
LOS ALAMOS, NM 85544
01CY ATTN DOC CON FOR J. BREEDLOVE

UNIVERSITY OF CALIFORNIA
LAWRENCE LIVERMORE LABORATORY
P.O. BOX 808
LIVERMORE, CA 94550
01CY ATTN DOC CON FOR TECH INFO DEPT
01CY ATTN DOC CON FOR L-389 R. OTT
01CY ATTN DOC CON FOR L-31 R. HAGER
01CY ATTN DOC CON FOR L-46 F. SEWARD

LOS ALAMOS NATIONAL LABORATORY
P.O. BOX 1663
LOS ALAMOS, NM 87545
01CY ATTN DOC CON FOR J. WOLCOTT
01CY ATTN DOC CON FOR R.F. TASCHEK
01CY ATTN DOC CON FOR E. JONES
01CY ATTN DOC CON FOR J. MALIK
01CY ATTN DOC CON FOR R. JEFFRIES
01CY ATTN DOC CON FOR J. ZINN
01CY ATTN DOC CON FOR P. KEATON
01CY ATTN DOC CON FOR D. WESTERVELT
01CY ATTN D. SAPPENFIELD

SANDIA LABORATORIES
P.O. BOX 5800
ALBUQUERQUE, NM 87115
01CY ATTN DOC CON FOR W. BROWN
01CY ATTN DOC CON FOR A. THORNBROUGH
01CY ATTN DOC CON FOR T. WRIGHT
01CY ATTN DOC CON FOR D. DAHLGREN
01CY ATTN DOC CON FOR 3141
01CY ATTN DOC CON FOR SPACE PROJECT DIV

SANDIA LABORATORIES
LIVERMORE LABORATORY
P.O. BOX 969
LIVERMORE, CA 94550
01CY ATTN DOC CON FOR B. MURPHEY
01CY ATTN DOC CON FOR T. COOK

OFFICE OF MILITARY APPLICATION
DEPARTMENT OF ENERGY
WASHINGTON, D.C. 20545
01CY ATTN DOC CON DR. YO SONG

OTHER GOVERNMENT

DEPARTMENT OF COMMERCE
NATIONAL BUREAU OF STANDARDS
WASHINGTON, D.C. 20234
01CY (ALL CORRES: ATTN SEC OFFICER FOR)

INSTITUTE FOR TELECOM SCIENCES
NATIONAL TELECOMMUNICATIONS & INFO ADMIN
BOULDER, CO 80303
01CY ATTN A. JEAN (UNCLASS ONLY)
01CY ATTN W. UTLAUT
01CY ATTN D. CROMBIE
01CY ATTN L. BERRY

NATIONAL OCEANIC & ATMOSPHERIC ADMIN
ENVIRONMENTAL RESEARCH LABORATORIES
DEPARTMENT OF COMMERCE
BOULDER, CO 80302
01CY ATTN R. GRUBB
01CY ATTN AERONOMY LAB G. REID

DEPARTMENT OF DEFENSE CONTRACTORS

AEROSPACE CORPORATION
P.O. BOX 92957
LOS ANGELES, CA 90009
01CY ATTN I. GARFUNKEL
01CY ATTN T. SALMI
01CY ATTN V. JOSEPHSON
01CY ATTN S. BOWER
01CY ATTN D. OLSEN

ANALYTICAL SYSTEMS ENGINEERING CORP
5 OLD CONCORD ROAD
BURLINGTON, MA 01803
01CY ATTN RADIO SCIENCES

AUSTIN RESEARCH ASSOC., INC.
1901 RUTLAND DRIVE
AUSTIN, TX 78758
01CY ATTN L. SLOAN
01CY ATTN R. THOMPSON

BERKELEY RESEARCH ASSOCIATES, INC.
P.O. BOX 983
BERKELEY, CA 94701
01CY ATTN J. WORCIAN
01CY ATTN C. PRETTIE
01CY ATTN S. BRECHT

BOEING COMPANY, THE
P.O. BOX 3707
SEATTLE, WA 98124
01CY ATTN G. KEISTER
01CY ATTN D. MURRAY
01CY ATTN G. HALL
01CY ATTN J. KENNEY

CHARLES STARK DRAPER LABORATORY, INC.
555 TECHNOLOGY SQUARE
CAMBRIDGE, MA 02139
01CY ATTN D.B. COX
01CY ATTN J.P. GILMORE

COMSAT LABORATORIES
LINTHICUM ROAD
CLARKSBURG, MD 20734
01CY ATTN G. HYDE

CORNELL UNIVERSITY
DEPARTMENT OF ELECTRICAL ENGINEERING
ITHACA, NY 14850
01CY ATTN D.T. FARLEY, JR.

ELECTROSPACE SYSTEMS, INC.
BOX 1359
RICHARDSON, TX 75080
01CY ATTN H. LOGSTON
01CY ATTN SECURITY (PAUL PHILLIPS)

EOS TECHNOLOGIES, INC.
606 Wilshire Blvd.
Santa Monica, Calif 90401
01CY ATTN C.B. GABBARD

ESL, INC.
495 JAVA DRIVE
SUNNYVALE, CA 94086
01CY ATTN J. ROBERTS
01CY ATTN JAMES MARSHALL

GENERAL ELECTRIC COMPANY
SPACE DIVISION
VALLEY FORGE SPACE CENTER
GODDARD BLVD KING OF PRUSSIA
P.O. BOX 8555
PHILADELPHIA, PA 19101
01CY ATTN M.H. BORTNER SPACE SCI LAB

GENERAL ELECTRIC COMPANY
P.O. BOX 1122
SYRACUSE, NY 13201
01CY ATTN F. REIBERT

GENERAL ELECTRIC TECH SERVICES CO., INC.
HMES
COURT STREET
SYRACUSE, NY 13201
01CY ATTN G. MILLMAN

GEOPHYSICAL INSTITUTE
UNIVERSITY OF ALASKA
FAIRBANKS, AK 99701
(ALL CLASS ATTN: SECURITY OFFICER)
01CY ATTN T.N. DAVIS (UNCLASS ONLY)
01CY ATTN TECHNICAL LIBRARY
01CY ATTN NEAL BROWN (UNCLASS ONLY)

GTE SYLVANIA, INC.
ELECTRONICS SYSTEMS GRP-EASTERN DIV
77 A STREET
NEEDHAM, MA 02194
01CY ATTN DICK STEINHOF

HSS, INC.
2 ALFRED CIRCLE
BEDFORD, MA 01730
01CY ATTN DONALD HANSEN

ILLINOIS, UNIVERSITY OF
107 COBLE HALL
150 DAVENPORT HOUSE
CHAMPAIGN, IL 61820
(ALL CORRES ATTN DAN MCCLELLAND)
01CY ATTN K. YEH

INSTITUTE FOR DEFENSE ANALYSES
1801 NO. BEAUREGARD STREET
ALEXANDRIA, VA 22311
01CY ATTN J.M. AEIN
01CY ATTN ERNEST BAUER
01CY ATTN HANS WOLFARD
01CY ATTN JOEL BENGSTON

INTL TEL & TELEGRAPH CORPORATION
500 WASHINGTON AVENUE
NUTLEY, NJ 07110
01CY ATTN TECHNICAL LIBRARY

JAYCOR
11011 TORREYANA ROAD
P.O. BOX 85154
SAN DIEGO, CA 92138
01CY ATTN J.L. SPERLING

JOHNS HOPKINS UNIVERSITY
APPLIED PHYSICS LABORATORY
JOHNS HOPKINS ROAD
LAUREL, MD 20810
01CY ATTN DOCUMENT LIBRARIAN
01CY ATTN THOMAS POTEMRA
01CY ATTN JOHN DASSOULAS

KAMAN SCIENCES CORP
P.O. BOX 7463
COLORADO SPRINGS, CO 80933
01CY ATTN T. MEAGHER

KAMAN TEMPO-CENTER FOR ADVANCED STUDIES
816 STATE STREET (P.O DRAWER QQ)
SANTA BARBARA, CA 93102
01CY ATTN DASIAC
01CY ATTN WARREN S. KNAPP
01CY ATTN WILLIAM MCNAMARA
01CY ATTN B. GAMBILL

LINKABIT CORP
10453 ROSELLE
SAN DIEGO, CA 92121
01CY ATTN IRWIN JACOBS

LOCKHEED MISSILES & SPACE CO., INC
P.O. BOX 504
SUNNYVALE, CA 94088
01CY ATTN DEPT 60-12
01CY ATTN D.R. CHURCHILL

LOCKHEED MISSILES & SPACE CO., INC.
3251 HANOVER STREET
PALO ALTO, CA 94304
01CY ATTN MARTIN WALT DEPT 52-12
01CY ATTN W.L. IMHOF DEPT 52-12
01CY ATTN RICHARD G. JOHNSON DEPT 52-12
01CY ATTN J.B. CLADIS DEPT 52-12

MARTIN MARIETTA CORP
ORLANDO DIVISION
P.O. BOX 5837
ORLANDO, FL 32805
01CY ATTN R. HEFFNER

M.I.T. LINCOLN LABORATORY
P.O. BOX 73
LEXINGTON, MA 02173
01CY ATTN DAVID M. TOWLE
01CY ATTN L. LOUGHLIN
01CY ATTN D. CLARK

MCDONNEL DOUGLAS CORPORATION
5301 BOLSA AVENUE
HUNTINGTON BEACH, CA 92647
01CY ATTN N. HARRIS
01CY ATTN J. MOULE
01CY ATTN GEORGE MROZ
01CY ATTN W. OLSON
01CY ATTN R.W. HALPRIN
01CY ATTN TECHNICAL LIBRARY SERVICES

MISSION RESEARCH CORPORATION
735 STATE STREET
SANTA BARBARA, CA 93101
01CY ATTN P. FISCHER
01CY ATTN W.F. CREVIER
01CY ATTN STEVEN L. GUTSCHE
01CY ATTN R. BOGUSCH
01CY ATTN R. HENDRICK
01CY ATTN RALPH KILB
01CY ATTN DAVE SOWLE
01CY ATTN F. FAJEN
01CY ATTN M. SCHEIBE
01CY ATTN CONRAD L. LONGMIRE
01CY ATTN B. WHITE

MISSION RESEARCH CORP.
1720 RANDOLPH ROAD, S.E.
ALBUQUERQUE, NEW MEXICO 87106
01CY R. STELLINGWERF
01CY M. ALME
01CY L. WRIGHT

MITRE CORPORATION, THE
P.O. BOX 208
BEDFORD, MA 01730
01CY ATTN JOHN MORGANSTERN
01CY ATTN G. HARDING
01CY ATTN C.E. CALLAHAN

MITRE CORP
WESTGATE RESEARCH PARK
1820 DOLLY MADISON BLVD
MCLEAN, VA 22101
01CY ATTN W. HALL
01CY ATTN W. FOSTER

PACIFIC-SIERRA RESEARCH CORP
12340 SANTA MONICA BLVD.
LOS ANGELES, CA 90025
01CY ATTN E.C. FIELD, JR.

PENNSYLVANIA STATE UNIVERSITY
IONOSPHERE RESEARCH LAB
318 ELECTRICAL ENGINEERING EAST
UNIVERSITY PARK, PA 16802
(NO CLASS TO THIS ADDRESS)
01CY ATTN IONOSPHERIC RESEARCH LAB

PHOTOMETRICS, INC.
4 ARROW DRIVE
WOBURN, MA 01801
01CY ATTN IRVING L. KOFSKY

PHYSICAL DYNAMICS, INC.
P.O. BOX 3027
BELLEVUE, WA 98009
01CY ATTN E.J. FREMOUW

PHYSICAL DYNAMICS, INC.
P.O. BOX 10367
OAKLAND, CA 94610
ATTN A. THOMSON

R & D ASSOCIATES
P.O. BOX 9695
MARINA DEL REY, CA 90291
01CY ATTN FORREST GILMORE
01CY ATTN WILLIAM B. WRIGHT, JR.
01CY ATTN ROBERT F. LELEVIER
01CY ATTN WILLIAM J. KARZAS
01CY ATTN H. ORY
01CY ATTN C. MACDONALD
01CY ATTN R. TURCO
01CY ATTN L. DeRAND
01CY ATTN W. TSAI

RAND CORPORATION, THE
1700 MAIN STREET
SANTA MONICA, CA 90406
01CY ATTN CULLEN CRAIN
01CY ATTN ED BEDROZIAN

RAYTHEON CO.
528 BOSTON POST ROAD
SUDBURY, MA 01776
01CY ATTN BARBARA ADAMS

RIVERSIDE RESEARCH INSTITUTE
330 WEST 42nd STREET
NEW YORK, NY 10036
01CY ATTN VINCE TRAPANI

SCIENCE APPLICATIONS, INC.
1150 PROSPECT PLAZA
LA JOLLA, CA 92037
01CY ATTN LEWIS M. LINSON
01CY ATTN DANIEL A. HAMLIN
01CY ATTN E. FRIEMAN
01CY ATTN E.A. STRAKER
01CY ATTN CURTIS A. SMITH
01CY ATTN JACK MCDOUGALL

SCIENCE APPLICATIONS, INC
1710 GOODRIDGE DR.
MCLEAN, VA 22102
ATTN: J. COCKAYNE

SRI INTERNATIONAL
333 RAVENSWOOD AVENUE
MENLO PARK, CA 94025
01CY ATTN DONALD NEILSON
01CY ATTN ALAN BURNS
01CY ATTN G. SMITH
01CY ATTN R. TSUNODA
01CY ATTN DAVID A. JOHNSON
01CY ATTN WALTER G. CHESNUT
01CY ATTN CHARLES L. RINO
01CY ATTN WALTER JAYE
01CY ATTN J. VICKREY
01CY ATTN RAY L. LEADABRAND
01CY ATTN G. CARPENTER
01CY ATTN G. PRICE
01CY ATTN R. LIVINGSTON
01CY ATTN V. GONZALES
01CY ATTN D. MCDANIEL

TECHNOLOGY INTERNATIONAL CORP
75 WIGGINS AVENUE
BEDFORD, MA 01730
01CY ATTN W.P. BOQUIST

TOYON RESEARCH CO.
P.O. Box 6890
SANTA BARBARA, CA 93111
01CY ATTN JOHN ISE, JR.
01CY ATTN JOEL GARBARINO

TRW DEFENSE & SPACE SYS GROUP
ONE SPACE PARK
REDONDO BEACH, CA 90278
01CY ATTN R. K. PLEBUCH
01CY ATTN S. ALTSCHULER
01CY ATTN D. DEE
01CY ATTN D/ STOCKWELL
SNTF/1575

VISIDYNE
SOUTH BEDFORD STREET
BURLINGTON, MASS 01803
01CY ATTN W. REIDY
01CY ATTN J. CARPENTER
01CY ATTN C. HUMPHREY

IONOSPHERIC MODELING DISTRIBUTION LIST
(UNCLASSIFIED ONLY)

PLEASE DISTRIBUTE ONE COPY TO EACH OF THE FOLLOWING PEOPLE (UNLESS OTHERWISE NOTED)

NAVAL RESEARCH LABORATORY
WASHINGTON, D.C. 20375
Dr. P. MANGE - CODE 4101
Dr. P. GOODMAN - CODE 4180

A.F. GEOPHYSICS LABORATORY
L.G. HANSCOM FIELD
BEDFORD, MA 01730
DR. T. ELKINS
DR. W. SWIDER
MRS. R. SAGALYN
DR. J.M. FORBES
DR. T.J. KENESHEA
DR. W. BURKE
DR. H. CARLSON
DR. J. JASPERSE

BOSTON UNIVERSITY
DEPARTMENT OF ASTRONOMY
BOSTON, MA 02215
DR. J. AARONS

CORNELL UNIVERSITY
ITHACA, NY 14850
DR. W.E. SWARTZ
DR. D. FARLEY
DR. M. KELLEY

HARVARD UNIVERSITY
HARVARD SQUARE
CAMBRIDGE, MA 02138
DR. M.B. McELROY
DR. R. LINDZEN

INSTITUTE FOR DEFENSE ANALYSIS
400 ARMY/NAVY DRIVE
ARLINGTON, VA 22202
DR. E. BAUER

MASSACHUSETTS INSTITUTE OF TECHNOLOGY
PLASMA FUSION CENTER
LIBRARY, NW16-262
CAMBRIDGE, MA 02139

NASA
GODDARD SPACE FLIGHT CENTER
GREENBELT, MD 20771
DR. K. MAEDA
DR. S. CURTIS
DR. M. DUBIN
DR. N. MAYNARD - CODE 696

COMMANDER
NAVAL AIR SYSTEMS COMMAND
DEPARTMENT OF THE NAVY
WASHINGTON, D.C. 20360
DR. T. CZUBA

COMMANDER
NAVAL OCEAN SYSTEMS CENTER
SAN DIEGO, CA 92152
MR. R. ROSE - CODE 5321

NOAA
DIRECTOR OF SPACE AND ENVIRONMENTAL LABORATORY
BOULDER, CO 80302
DR. A. GLENN JEAN
DR. G.W. ADAMS
DR. D.N. ANDERSON
DR. K. DAVIES
DR. R.F. DONNELLY

OFFICE OF NAVAL RESEARCH
800 NORTH QUINCY STREET
ARLINGTON, VA 22217
DR. G. JOINER

PENNSYLVANIA STATE UNIVERSITY
UNIVERSITY PARK, PA 16802
DR. J.S. NISBET
DR. P.R. ROHRBAUGH
DR. L.A. CARPENTER
DR. M. LEE
DR. R. DIVANY
DR. P. BENNETT
DR. F. KLEVANS

SCIENCE APPLICATIONS, INC.
1150 PROSPECT PLAZA
LA JOLLA, CA 92037
DR. D.A. HAMLIN
DR. E. FRIEMAN

STANFORD UNIVERSITY
STANFORD, CA 94305
DR. P.M. BANKS

U.S. ARMY ABERDEEN RESEARCH
AND DEVELOPMENT CENTER
BALLISTIC RESEARCH LABORATORY
ABERDEEN, MD
DR. J. HEIMERL

GEOPHYSICAL INSTITUTE
UNIVERSITY OF ALASKA
FAIRBANKS, AK 99701
DR. L.E. LEE

UNIVERSITY OF CALIFORNIA,
BERKELEY
BERKELEY, CA 94720
DR. M. HUDSON

UNIVERSITY OF CALIFORNIA
LOS ALAMOS SCIENTIFIC LABORATORY
J-10, MS-664
LOS ALAMOS, NM 87545
DR. M. PONGRATZ
DR. D. SIMONS
DR. G. BARASCH
DR. L. DUNCAN
DR. P. BERNHARDT
DR. S.P. GARY

UNIVERSITY OF MARYLAND
COLLEGE PARK, MD 20740
DR. K. PAPADOPOULOS
DR. E. OTT

JOHNS HOPKINS UNIVERSITY
APPLIED PHYSICS LABORATORY
JOHNS HOPKINS ROAD
LAUREL, MD 20810
DR. R. GREENWALD
DR. C. MENG

UNIVERSITY OF PITTSBURGH
PITTSBURGH, PA 15213
DR. N. ZABUSKY
DR. M. BIONDI
DR. E. OVERMAN

UNIVERSITY OF TEXAS
AT DALLAS
CENTER FOR RESEARCH SCIENCES
P.O. BOX 688
RICHARDSON, TX 75080
DR. R. HEELIS
DR. W. HANSON
DR. J.P. McCLURE

UTAH STATE UNIVERSITY
4TH AND 8TH STREETS
LOGAN, UTAH 84322
DR. R. HARRIS
DR. K. BAKER
DR. R. SCHUNK
DR. J. ST.-MAURICE

PHYSICAL RESEARCH LABORATORY
PLASMA PHYSICS PROGRAMME
AHMEDABAD 380 009
INDIA
P.J. PATHAK, LIBRARIAN

LABORATORY FOR PLASMA AND
FUSION ENERGY STUDIES
UNIVERSITY OF MARYLAND
COLLEGE PARK, MD 20742
JHAN VARYAN HELLMAN,
REFERENCE LIBRARIAN

END

FILMED

4-84

DTIC